

# *Spatial and temporal variations of the seasonal sea level cycle in the northwest Pacific*

Article

Accepted Version

Feng, X. ORCID: <https://orcid.org/0000-0003-4143-107X>, Tsimplis, M. N., Marcos, M., Calafat, F. M., Zheng, J., Jorda, G. and Cipollini, P. (2015) Spatial and temporal variations of the seasonal sea level cycle in the northwest Pacific. *Journal of Geophysical Research: Oceans*, 120 (10). pp. 7091-7112. ISSN 2169-9291 doi: 10.1002/2015JC011154 Available at <https://centaur.reading.ac.uk/44451/>

It is advisable to refer to the publisher's version if you intend to cite from the work. See [Guidance on citing](#).

Published version at: <http://onlinelibrary.wiley.com/doi/10.1002/2015JC011154/abstract>

To link to this article DOI: <http://dx.doi.org/10.1002/2015JC011154>

Publisher: American Geophysical Union

All outputs in CentAUR are protected by Intellectual Property Rights law, including copyright law. Copyright and IPR is retained by the creators or other copyright holders. Terms and conditions for use of this material are defined in the [End User Agreement](#).

[www.reading.ac.uk/centaur](http://www.reading.ac.uk/centaur)

**CentAUR**

Central Archive at the University of Reading

Reading's research outputs online

1

2   **Spatial and temporal variations of the seasonal sea level cycle in**  
3   **the northwest Pacific**

4

5   Xiangbo Feng<sup>1,2,3\*</sup>, Michael N. Tsimplis<sup>2</sup>, Marta Marcos<sup>4</sup>, Francisco M. Calafat<sup>2</sup>,

6   Jinhai Zheng<sup>3</sup>, Gabriel Jordà <sup>4</sup> and Paolo Cipollini<sup>2</sup>

7

8   1. Department of Meteorology, University of Reading, Reading, UK

9   2. National Oceanography Centre, Southampton, UK

10   3. Hohai University, Nanjing, China

11   4. IMEDEA (CSIC–UIB), Esporles, Spain

12

13   \* Corresponding author: Xiangbo Feng (xiangbo.feng@reading.ac.uk)

14

15

## 16    **Abstract**

17    The seasonal sea level variations observed from tide gauges over 1900-2013 and  
18    gridded satellite altimeter product AVISO over 1993-2013 in the northwest  
19    Pacific have been explored. The seasonal cycle is able to explain 60-90% of  
20    monthly sea level variance in the marginal seas, while it explains less than 20%  
21    of variance in the eddy-rich regions. The maximum annual and semi-annual sea  
22    level cycles (30cm and 6cm) are observed in the north of the East China Sea and  
23    the west of the South China Sea respectively. AVISO was found to underestimate  
24    the annual amplitude by 25% compared to tide gauge estimates along the coasts  
25    of China and Russia.

26    The forcing for the seasonal sea level cycle was identified. The atmospheric  
27    pressure and the steric height produce 8-12cm of the annual cycle in the middle  
28    continental shelf and in the Kuroshio Current regions separately. The removal of  
29    the two attributors from total sea level permits to identify the sea level residuals  
30    that still show significant seasonality in the marginal seas. Both nearby wind  
31    stress and surface currents can explain well the long-term variability of the  
32    seasonal sea level cycle in the marginal seas and the tropics because of their  
33    influence on the sea level residuals. Interestingly, the surface currents are a  
34    better descriptor in the areas where the ocean currents are known to be strong.  
35    Here, they explain 50-90% of inter-annual variability due to the strong links  
36    between the steric height and the large-scale ocean currents.

37



## 38    **1. Introduction**

39    The seasonal cycle, and more specifically its annual and semi-annual  
40    components, dominates the non-tidal variability of sea level in many regions of  
41    the ocean. Because the seasonal variability is very energetic for monthly sea level  
42    records and also it is auto-correlated, this signal is normally removed from the  
43    estimation of trends of mean sea level. However, this does not hide the practical  
44    significance of the seasonal cycle. Coastal infrastructure is more vulnerable at the  
45    time when the seasonal sea level cycle is at its highest [*Tsimplis and Shaw, 2010*;  
46    *Dangendorf et al., 2013a; Torres and Tsimplis, 2014*], and the decadal increases in  
47    the seasonal cycle will make the vulnerability of the coastal areas even higher.  
48    The seasonal changes in stratification, which are seen in the seasonal sea level  
49    cycle, can cause significant seasonal changes in tides [*Kang et al., 2002; Müller et*  
50    *al., 2014*], leading to the prediction of tides and extremes more complicated.  
51    Furthermore, the seasonal sea level cycle is firmly regulating the seawater-  
52    freshwater balance both under the ground [*Michael, et al., 2005*] and at the river  
53    estuaries [*Anderson and Lockaby, 2012*], and it acts as a key factor determining  
54    the seawater intrusion. Therefore, obtaining good physical understanding of the  
55    processes involved in determining the seasonal sea level cycle and its spatial and  
56    temporal changes enables us to assess the extent of future changes in climate  
57    that will impact on the coastal ocean environments.

58    The gravitational forcing contributes very little (in mm) to the observed seasonal  
59    sea level cycle [*Pugh and Woodworth, 2014*]. Seasonality in meteorological,  
60    oceanographic and hydrological processes is considered to force the seasonal sea  
61    level cycle, but the contribution of each factor varies spatially and temporally

62 [Plag and Tsimplis, 1999; Marcos and Tsimplis, 2007; Hünicke and Zorita, 2008;  
63 Vinogradov et al., 2008; Torres and Tsimplis, 2012; Dangendorf et al., 2013b;  
64 Wahl et al., 2014]. Notably, temporal changes in the seasonal sea level cycle may  
65 be caused by the sea level components which are not the dominant ones.  
66 Therefore, mapping the seasonal sea level cycle, identifying the dominant  
67 components regionally and furthermore identifying the forcing of its temporal  
68 changes is very important in order to understand the physics of the sea level  
69 variability at the seasonal frequencies.

70 On the basis of tide gauge data, Tsimplis and Woodworth [1994] mapped the  
71 features of the seasonal sea level cycle in coastal waters, showing spatial  
72 variability but also regional coherence. Satellite radar altimetry has the  
73 capability of monitoring the sea level variations with a better spatial coverage,  
74 and the native altimetric along-track data are often gridded for further use of  
75 analysis and visualization. Chen et al. [2000] explored the estimations of the  
76 seasonal cycle in open oceans using gridded altimeter measurements. However,  
77 at the continental coasts the altimetry was found to significantly underestimate  
78 the annual level cycle [Han and Huang, 2008; Vinogradov and Ponte, 2010]. This  
79 underestimation is normally caused by a combination of data flagging (in turn  
80 due to contamination of the altimetric waveforms and/or inadequacy of some of  
81 the corrections such as the one compensating for path delay due to water vapour)  
82 and data filtering in the last 20-30 km from the coasts. For the gridded altimeter  
83 data, the mapping procedure additionally tends to smooth the characteristics of  
84 the local phenomena of sea level that are captured by the tide gauges. For each  
85 region, it is vital to clearly identify the uncertainty of the altimeter products in

86 estimating the seasonal sea level before using their results into other fields. It is  
87 worth noting that considerable research efforts are being put into improving the  
88 along-track altimetry in the coastal zone [*Vignudelli et al.*, 2011]. The latest  
89 coastal altimetry products reprocessed with improved techniques allow a better  
90 representation of sea level variability near the coasts [*Passaro et al.*, 2015] but  
91 those products are not yet available for all the past missions and coastal areas  
92 and therefore time series are limited.

93 The stability of the seasonal sea level cycle with time has also been studied for a  
94 few regions where long-term tide gauge records exist. The annual cycle  
95 amplitude was found to exhibit decadal variations between 1 to 20 cm in the  
96 European coasts [*Plag and Tsimplis*, 1999; *Barbosa et al.*, 2008; *Hünicke and*  
97 *Zorita*, 2008; *Dangendorf et al.*, 2013b], the Mediterranean Sea [*Marcos and*  
98 *Tsimplis*, 2007], the Caribbean Sea [*Torres and Tsimplis*, 2012] and the South  
99 China Sea [*Amiruddin et al.*, 2015]. Interestingly, the annual cycle amplitude  
100 along the US Gulf coast was recently reported to have increased by 20-30% since  
101 1990s, and the sea surface air temperature was argued as an indicator for the  
102 increase [*Wahl et al.*, 2014]. These studies are all based on the traditional annual  
103 cycle definitions, assuming that both amplitude and frequency of the annual  
104 cycle are constant within each time segment of assessments but that they are  
105 allowed to change over different segments. Consequently, there is a possibility  
106 that the inter-annual or even lower-frequency variability in the monthly values  
107 may be treated as part of the annual cycle signal if the length of assessment  
108 windows is not appropriate. An alternative method, the modulated annual cycle  
109 that allows the annual cycle parameters to change instantaneously, was

110 introduced to the climate analysis by *Wu et al.* [2008]. Based on this concept,  
111 some reconstruction products have been made to recover the high- and low-  
112 frequency signals in sea level [*Hamlington et al.*, 2010, 2011 and 2012].

113 The northwest Pacific is a region where both oceanographic and atmospheric  
114 dynamics (e.g. the western boundary currents, the monsoon and typhoons) are  
115 known to have strong impacts on the sea surface processes. The areas studied  
116 here are of particular interest also because they are heavily populated areas  
117 where intensive anthropogenic activities were found to have significantly  
118 changed the coastal geomorphology [*Wang et al.*, 2014, and references therein].  
119 *Marcos et al.* [2012] identified the spatial and temporal variations of mean sea  
120 level in the marginal seas of this region and associated them with the large-scale  
121 climatic variability. *Feng et al.* [2015] explored the long-term changes in tidal  
122 signals and proposed them as the consequences of the anthropogenic activities.  
123 These sea level components were suggested to consequently alter the  
124 occurrence of extremes [*Feng and Tsimplis*, 2014]. However, the seasonal cycle,  
125 as a crucial component in sea level, has not been systematically studied over the  
126 whole region of the northwest Pacific. The dynamics behind the spatial and  
127 temporal variations remain unrevealed.

128 This paper provides a regional investigation on the seasonal sea level cycle over  
129 the northwest Pacific, by using publically accessible datasets, which include tide  
130 gauge records, gridded satellite altimetry data and atmospheric and oceanic  
131 reanalysis. Four questions are addressed. Firstly, what are the spatial features of  
132 the seasonal sea level cycle in this region; secondly, to what extent can gridded  
133 satellite altimetry product estimate the coastal seasonal sea level cycle; thirdly,

134 how much do the seasonal signals change with time; and fourthly, what are the  
135 causes for the seasonal sea level oscillations and for their long-term variability as  
136 well, and to what extent can each of the contributors explain the variability.

137 The paper is structured as follows. In section 2, the data processing of sea level  
138 observations and atmospheric and oceanic climate reanalysis used are described  
139 together with the methodologies. In Section 3, spatial features of the seasonal sea  
140 level cycle are investigated, and harmonic parameters estimated from tide  
141 gauges and gridded altimetry data are compared. Temporal variability of the  
142 seasonal cycle is also addressed in this section. In Section 4, mechanisms for the  
143 spatial and temporal changes of the seasonal sea level cycle are explored,  
144 including the atmosphere pressure loading, the ocean thermal  
145 expansion/contraction and freshwater content, the wind stress and the sea  
146 surface currents. Finally, the conclusions are given in Section 5.

147

## 148 **2. Data and methodology**

### 149 **2.1 Sea level observational records**

150 Monthly sea level data ( $\eta$ ) recorded at 120 tide gauges in the northwest Pacific  
151 were obtained from the Permanent Service for Mean Sea Level [*Holgate et al.*,  
152 2013]. Locations and numbering of the 120 tide gauge stations are provided in  
153 **Figure 1a**. Tide gauges are classified into 6 sub-regions: the east of the South  
154 China Sea (SCS-E) (station number: 1-14), the west of the South China Sea (SCS-  
155 W) (station number: 15-39), the East China Sea (ECS) (station number: 40-61),

156 the Sea of Japan (SoJ) (station number: 62-89), the northeast coasts of Japan  
157 (Japan-NE) (station number: 90-105) and the southeast coasts of Japan (Japan-  
158 SE) (station number: 106-115). There are two stations on the coasts of the Sea of  
159 Okhotsk (station number: 119 and 120) and three stations in the south of Japan  
160 (station number: 116-118) where the observed seasonal sea level cycle has  
161 different behaviour from that at neighboring sites (this will be discussed in  
162 subsection 3.3). Thus, these five stations are taken as outliers relative to above 6  
163 sub-regions. The dataset used spans the period 1900-2013. However, only a few  
164 stations have records longer than 50 years (**Figure 1b**). The minimum record  
165 length used in the analysis was 16 years. The dataset contains 105 revised local  
166 reference records and 15 metric records. The metric records do not contain the  
167 information about the benchmark datum contributed by re-leveling adjustments  
168 to a certain level, but they can be useful for studies of the seasonal sea level cycle  
169 if they are carefully treated.

170 The data quality control of tide gauge records performed included the visual  
171 checks of time series and the adjustment or removal of values over periods with  
172 spurious shifts. Although it is not necessary to know the actual level of the datum  
173 for estimating the seasonal cycle, the stability of the datum is still important for  
174 assessing the temporal variability of the cycle. Where a record showed datum  
175 shifts over different segments these were adjusted to the same reference level by  
176 removing their mean values after each segment was detrended. Sea level values  
177 that showed obvious jumps or shifts after the known earthquakes were also  
178 excluded. Two massive earthquakes were considered, which stroke the Kuril  
179 Islands on the 4<sup>th</sup> October 1994 and the Oshika Peninsula on the 11<sup>th</sup> March 2011

180 respectively ([www.nodc.noaa.gov/outreach/esm](http://www.nodc.noaa.gov/outreach/esm)). For individual records, mean  
 181 values and trends were removed and then plotted into 6 groups as specified  
 182 above. In each group, if parts of records show spurious jumps or shifts compared  
 183 with other members, or go beyond the spreading edges of the ensembles, these  
 184 records are omitted. **Figure 1b** gives the period of valid data at each station after  
 185 the quality control.

186 Gridded satellite radar altimeter data that cover the northwest Pacific (0-65°N,  
 187 100°E -170°E) were also used. The data were produced by SSALTO/DUACS and  
 188 distributed by AVISO, with support from CNES  
 189 (<http://www.aviso.altimetry.fr/duacs/>). The data consist of monthly averaged  
 190 maps of sea level anomalies, corresponding to multimission gridded sea surface  
 191 height anomaly (including Saral, Cryosat-2, Jason-1&2, T/P, Envisat, GFO, ERS-  
 192 1&2 and Geosat) with respect to a 21-year mean sea level. The spatial resolution  
 193 of the gridded altimeter data is  $1/4^\circ \times 1/4^\circ$ , which permits resolving the sea  
 194 level related to the mesoscale eddies. Oceanic and atmospheric dynamics are  
 195 routinely corrected in the mission track data. These include the ocean tide, the  
 196 pole tide and the dynamic atmospheric correction (DAC) [Carrère and Lyard,  
 197 2003]. Because the inverted barometer (IB) effect ( $\eta_{IB}$ ) has been corrected in the  
 198 AVISO data, we here refer to the monthly sea level records from AVISO as  $\eta - \eta_{IB}$ .

## 199 **2.2 Atmospheric pressure data and the IB effect**

200 In the open ocean, the sea level is assumed to isostatically react to the  
 201 atmospheric pressure loading on the sea surface by the inverted barometer (IB)  
 202 effect ( $\eta_{IB}$ ) [Gill, 1982; Wunsch and Stammer, 1997; Ponte, 2006].  $\eta_{IB} = -1/\rho g(P-$

203  $P_{ref}$ ), where  $\rho$  and  $g$  are the water density and gravity acceleration respectively,  
204 and  $P - P_{ref}$  is the fluctuation of sea level pressure  $P$  relative to a long-term  
205 average  $P_{ref}$  over the global ocean [Wunsch and Stammer, 1997; Ponte, 2006].  
206 The consequence of a 1-mbar increase in surface pressure is approximately 1cm  
207 depression of sea level.

208 With respect to the tide gauge records, the monthly sea level pressure data over  
209 1900-2013 were used to calculate  $\eta_{IB}$  closest to the stations. The pressure data  
210 were obtained by combining the NOAA's 20<sup>th</sup> century reanalysis v2 for the  
211 period 1900-2012 [Compo et al., 2011] and the ECMWF-Interim for 2013. Please  
212 note that for each tide gauge record  $\eta_{IB}$  is only applied over the periods when  
213 the tide gauge has valid data.

214 For AVISO records, the monthly average of 6-hour dynamic atmospheric  
215 corrections (DAC) was used as  $\eta_{IB}$  over the sea surface. The DAC data are the sea  
216 level variability combining the high-frequency signals (less than 20 days) due to  
217 atmospheric wind and pressure forcing and low-frequency signals (more than 20  
218 days) from the static IB correction on the atmospheric pressure. The monthly  
219 average of DAC is equivalent to the isostatic IB effect [Pascual et al., 2008]. The  
220 DAC data are produced by CLS Space Oceanography Division using the Mog2D  
221 model from Legos [Carrère and Lyard, 2003] and distributed by AVISO.

### 222 **2.3 Ocean temperature and salinity analysis and the steric height**

223 The steric height was calculated from the 3D hydrographic gridded product  
224 EN4.0.2 generated by the UK Met Office Hadley Centre. This product has been  
225 generated through the objective analysis of a global quality controlled dataset of



226 ocean temperature and salinity profiles, and is provided on a grid with 1° spatial  
 227 resolution in the horizontal and 42 levels in the vertical [Good *et al.*, 2013]  
 228 covering the period 1900-2013. The main observational data source is WOD09  
 229 [Boyer *et al.*, 2009]. The steric component of seasonal sea level change is mainly  
 230 due to the water density changes over the thermocline depth [Chen *et al.*, 2000;  
 231 Vinogradov *et al.*, 2008; Torres and Tsimplis, 2012]. Therefore, the values over  
 232 the top 500m were used in the calculation of the steric signal.

233 The steric height ( $\eta_{ster}$ ), consisting of thermosteric ( $\eta_{thermo}$ ) and halosteric  
 234 components ( $\eta_{halo}$ ), over water depth ( $H$ ) can be expressed as:

$$\eta_{thermo} = \int_{-H}^0 C \cdot \Delta T dz \quad (1)$$

$$\eta_{halo} = \int_{-H}^0 D \cdot \Delta S dz$$

235 where  $\Delta T$  and  $\Delta S$  are the temperature and salinity fluctuation relative to the  
 236 mean values over the whole period of study at each layer, and  $C$  and  $D$  are the  
 237 thermal expansion and salt compression coefficients respectively [Tabata, 1986].  
 238  $C$  and  $D$  are defined as

$$C = -\frac{1}{\rho} \frac{\partial \rho}{\partial T}$$

$$D = -\frac{1}{\rho} \frac{\partial \rho}{\partial S} \quad (2)$$

239 where  $\rho$  is the water density, depending on water depth, temperature and  
240 salinity, and is defined by the Joint Panel on Oceanographic Tables and Standards  
241 [UNESCO, 1981].

242  $\eta_{ster}$  calculated at tide gauge stations or shallow water regions is usually very  
243 small and cannot represent the entire seasonal steric signal. Thus we used the  
244 values at deep grid points (over 500m) closest to the sites of interest. This  
245 method assumes that the whole steric signal in the deep ocean is transmitted to  
246 the coast [Bingham and Hughes, 2012].

247 We also repeated the above process to calculate  $\eta_{ster}$  based in the 3D gridded  
248 oceanic properties from the Simple Ocean Data Assimilation (SODA), which will  
249 be introduced later, in order to explain the mechanisms of the long-term  
250 variations of the seasonal sea level cycle.

## 251 **2.4 Ocean reanalysis SODA**

252 The sea surface height without the IB effect ( $\eta - \eta_{IB}$ ), 3D ocean temperature and  
253 salinity, the wind stress and the sea surface currents from the Simple Ocean Data  
254 Assimilation (SODA) v2.2.4 covering the period 1900-2010 were also used to  
255 understand the forcing of the seasonal sea level cycle. The SODA reanalysis is  
256 based on the Parallel Ocean Program ocean model [Smith *et al.*, 1992], with  $0.25^\circ$   
257  $\times 0.4^\circ$  horizontal resolution and 40 vertical levels, and assimilates oceanic data  
258 through an optimal interpolation method every 10 days [Carton *et al.*, 2000]. In  
259 the version v2.2.4 [Giese and Ray, 2011], the observations used in the data  
260 assimilation scheme only include the ocean temperature and salinity profiles  
261 from WOD09 [Boyer *et al.*, 2009] (it is also the main data source for the Met

Office Hadley Centre EN4) and sea surface temperature from ICOADS 2.5 [Woodruff *et al.*, 2011]. Thus, SODA is expected to be able to seasonally represent the steric height in sea level. It is worth noting that SODA does not assimilate sea level observations (i.e. from altimetry or tide gauges). The model is forced with atmospheric fields from the NOAA's 20<sup>th</sup> century reanalysis v2 [Compo *et al.*, 2011] over the period 1871-2010 [Carton and Giese, 2008]

We use SODA for the purpose of identifying the forcing of the seasonal sea level cycle (the method used in estimating the seasonal sea level cycle will be described in the next subsection). To do so it is necessary to first assess the capability of SODA in describing the observed seasonal sea level cycle in this region. Please note that because SODA does not include the IB effect, in the assessment  $\eta_{IB}$  was excluded both in AVISO data and in tide gauge records, ensuring that the three datasets are all free of the IB effect. Details of the assessment are provided in the supplementary materials. The comparison results are summarized as: 1) the mean seasonal sea level cycle determined by SODA over 1993-2010 is in good agreement with the estimations observed by AVISO over 1993-2013 in most areas, with some discrepancies for annual amplitudes below 3-6 cm and mainly occurring at the coastal regions (**Figure S1-S2**); 2) the inter-annual variability of the seasonal sea level cycle over 1900-2010 from SODA has significant correlation with the results observed at most of the tide gauge records (in 96 of 120), with  $R=0.59$  and  $0.58$  on average for annual and semi-annual amplitudes respectively, and the worse representation of SODA is mainly in the north of East China Sea and the north of the Sea of Japan where the tide gauge records are relatively short (**Figure S3**); and 3) when the regional

average is concerned, SODA can well represent the inter-annual variability of the seasonal sea level cycle for each sub-region (**FigureS4**), with correlation  $R=0.61$  and  $0.57$  on average for annual and semi-annual amplitudes against tide gauge observations. Thus, we conclude that SODA reproduces the seasonal sea level cycle in the area of study with a reasonable accuracy and we will use it in the characterization of the forcing mechanisms that determine the seasonal cycle.

It should be kept in mind that discrepancies of SODA still exist in the seasonal sea level cycle estimations. This can be due to many different aspects of SODA, such as the quality of atmospheric forcing, the low resolutions of the model at coasts, the non-conserving global water mass [Tamisiea *et al.*, 2010], or the non-conserving budgets in the ocean data assimilation procedure [Haines *et al.*, 2012]. More efforts are needed to interpret the skills of SODA, but this is not the scope of this paper.

## 2.5 Regression model for seasonal cycle

The harmonic parameters of the annual and semi-annual cycles were estimated through least squares fitting to the monthly records by the following equation:

$$\eta(t) = \beta_0 + A_a \cos\left(\frac{2\pi}{12}(t - \phi_a)\right) + A_{sa} \cos\left(\frac{2\pi}{6}(t - \phi_{sa})\right) \quad (3)$$

where  $\eta(t)$  is the monthly mean value of sea level at time  $t$  (in units of months and corresponding to the middle of January),  $\beta_0$  is the estimated mean value, and  $A_a$  and  $A_{sa}$  are the annual and semi-annual amplitudes corresponding to the phase lags of  $\phi_a$  and  $\phi_{sa}$  respectively. The significance of the estimated harmonic

parameters was tested at 95% confidence level by assuming the regression errors are normally distributed. Note that all the monthly records used in the analysis were detrended over the period before being fitted by Eq.(3).

The mean seasonal cycle for each sea level record was estimated on the basis of Eq. (3) using the data over the whole period. The temporal variability of the seasonal cycle was also estimated on the basis of applying Eq. (3) for 5-year segments shifted year-by-year. The 5-year length of data segment was chosen as suggested by *Tsimplis and Woodworth* [1994] as a period over which most records provide stable estimates for the seasonal cycle.

We applied this method to different sea level components, the wind stress and the sea surface currents, to diagnose the forcing mechanisms of the seasonal sea level cycle. In estimating the temporal variability of the seasonal cycle for the wind stress and the sea surface currents, the two variables as 2D vectors are equally divided into 18 sections (0-180° relative to the east anticlockwise by 10°) to get their values at different directions. This process permits us to distinguish the vectors with the direction that have the best correlations with the seasonal sea level variations.

### **3. Seasonal sea level cycle from observations**

#### **3.1 Monthly sea level variations**

The monthly variances of  $\eta$  from tide gauges and AVISO are shown in **Figure 2a**. Note that  $\eta$  from AVISO is obtained by adding  $\eta_{IB}$  (DAC data) back to  $\eta - \eta_{IB}$  (AVISO sea level records). The variance exceeds 300 cm<sup>2</sup> in the north of the East

329 China Sea and in regions with strong western boundary currents, i.e. the  
330 Kuroshio Extension and the south Oyashio Currents. Values of 150-200 cm<sup>2</sup> are  
331 found in the East China Sea, the Luzon Strait, the Gulf of Thailand and the area of  
332 the Equatorial Current.

333 **Figure 2b** shows the percentage of variance explained by the seasonal cycle  
334 regression model of Eq.(3). The regression model explains 60-90% of the  
335 variance in the vast majority of areas of the marginal seas over the continental  
336 shelf, except in the Sea of Okhotsk where sea ice usually exists in cold seasons  
337 [Parkinson *et al.*, 1999]. In the open ocean the percentage of variance explained  
338 by the seasonal cycle is very low, except in a zonal band (10°N -20°N) and in the  
339 west of the ocean interior where 40-50% of sea level variance can be attributed  
340 to the seasonal cycle. It is worth noting that in the regions of the Kuroshio  
341 Extension and the south Oyashio Currents, where the sea level variance is  
342 maximum (**Figure 2a**), the seasonal cycle captures less than 20% of variance  
343 (**Figure 2b**). The low representativeness of the seasonal cycle in the open ocean  
344 can be interpreted by the presence of eddies which have the strong signature in  
345 sea level (and thus induce high variance in sea level observations) but which  
346 usually have much irregular seasonal variations. In fact, this region has been  
347 identified as the region with the richest mesoscale eddies in the world [Chelton *et*  
348 *al.*, 2011].

349 The sea level variance observed by AVISO at the closest points to tide gauges is  
350 lower than that observed by tide gauges at 96 of the 120 stations. The difference  
351 of variance (AVISO – tide gauges) is -31 cm<sup>2</sup> on average (21% of variance  
352 determined by tide gauges). The largest discrepancies occur in the north of the

Philippines and at the west of the South China Sea (**Figure 2a**). When the period of AVISO (1993-2013) is considered, there are 103 tide gauge records having valid data over the period. AVISO is then found to underestimate the sea level variance again at 64 of the 103 stations by overall  $-16 \text{ cm}^2$  (11% of variance by tide gauges). Thus, we conclude that AVISO underestimates the coastal sea level variance at most of stations disregarding the period.

In the estimations, the annual and semi-annual cycle parameters in Eq.(3) are assumed to be constant during the whole period of records. Actually, as we will discuss later, they could change in time. Thus, we cannot rule out the possibility that the sea level variance accounted by the seasonal cycle and the resulting percentages as indicated above may change when different periods of time are considered.

### 3.2 Mean seasonal sea level cycle

The annual cycle of  $\eta$  is significant at all tide gauge records and in most areas (**Figure 3a-b**). The values of  $A_a$  exceed 15cm in the East China Sea, the south of Japan, the areas of the Kuroshio Current, the Luzon Strait and the Gulf of Thailand.  $A_a$  is less than 3cm or becomes statistically insignificant in the equator area (0-10°N) and the Sea of Okhotsk. The highest  $A_a$  ( $29 \pm 1 \text{ cm}$ ) occurs at the north of the East China Sea (station number: 47 and 48). The annual phase  $\phi_a$  is in December-January in the equator area, while it changes to August-November when heading to north.  $\phi_a$  is not uniform in each basin, except in the East China Sea.

375 The semi-annual cycle is significant at most of tide gauge records (113 of 120), in  
376 the equator area and in most areas of marginal seas, except in the Sea of Japan  
377 **(Figure 3c-d)**.  $A_{sa}$  has the highest values of 5-7cm in the northwest of the South  
378 China Sea and in the Kuroshio Extension area.  $\phi_{sa}$  is changing from January to  
379 May (or July to November) when heading to south, and the direction of  $\phi_{sa}$   
380 change is in opposite to that of  $\phi_a$  change **(Figure 3b)**.

381 The comparisons of the annual and semi-annual parameters derived from AVISO  
382 and tide gauge measurements are shown in **Figure 4**. The differences are  
383 regarded as significant if the error bars of the two compared values do not  
384 overlap. At the points closest to tide gauges, AVISO significantly underestimates  
385  $A_a$  at 59 of the 120 stations by 2-9cm, with 3.5cm on average (25% of tide  
386 gauges estimates), and overestimates at 2 stations (station number: 6 and 93) by  
387 1.4cm and 2.2cm (37% and 42% of tide gauge estimates) **(Figure 4a)**. Large  
388 underestimations of 5-8cm (~40% of tide gauges values) are found in the west of  
389 the South China Sea, the East China Sea and the Sea of Japan. Meanwhile,  $\phi_a$   
390 derived from AVISO is significantly advanced by 10-35 days at 18 stations and  
391 delayed by 5-12 days at 4 stations **(Figure 4b)**. The semi-annual cycle is  
392 detectable at 113 stations for tide gauge measurements but only detectable at  
393 the corresponding AVISO points for 87 stations. AVISO underestimates  $A_{sa}$  by 1-  
394 3cm (60%) at 28 of the 87 stations, while discrepancies of  $\phi_{sa}$  occur at only 8  
395 stations when the error bars are considered **(Figure 4c-d)**.

396 The discrepancies of the seasonal sea level cycle estimated from AVISO still  
397 remain when the common period (1993-2013) is used at tide gauge records for  
398 the comparisons. We also found that the differences of harmonic parameters



399 derived from AVISO and tide gauges can well explain the discrepancies of the sea  
400 level variance in most of the coastal areas, which have been identified in  
401 subsection 3.1. This indicates that the underestimation of the seasonal cycle  
402 amplitudes is consistent with the errors of the sea level variance. Therefore, we  
403 confirm that the discrepancies of sea level seasonality identified between the  
404 two datasets are real and are not due to the methods used in the estimation.

### 405 **3.3 Temporal variability of the seasonal sea level cycle**

406 The temporal variability of the seasonal sea level cycle is produced by fitting  
407 Eq.(3) into a 5-year segment of tide gauge records ( $\eta$ ) with year-by-year shifting.  
408 **Figure 5** shows the inter-annual variations of the seasonal sea level amplitudes  
409 with respect to their own mean amplitudes for each station in the 6 sub-regions  
410 (gray lines in the figure). The temporal changes for 5 outlier stations (station  
411 number: 116-120) are provided in the supplementary material (**Figure S5**), and  
412 at these stations the seasonal sea level cycle shows different temporal variability  
413 in relation to the 6 sub-regions. Regional averages of the temporal changes in the  
414 seasonal cycle are obtained by averaging all seasonal cycle amplitude anomalies  
415 in one sub-region (black bold lines in **Figure 5**).

416 The annual and semi-annual sea level cycles are not constant in time (**Figure 5**).  
417 The range between maximum and minimum  $A_a$  at individual stations usually  
418 varies from 2cm to 8.6cm, with an average of 4.2cm (33% of their maximum  
419 amplitudes). The largest ranges of 20.4cm and 16.5cm are observed at two  
420 outliers in the south of Japan (station number: 116 and 117, see Figure S5). In  
421 spite of apparent regional features, the inter-annual variability of  $A_a$  also shows

some consistency among regions. In particular, the significant change by  $\sim 4$  cm for regional averages of  $A_a$  in the 1990's was present in all the regions. The range of  $A_{sa}$  differences over time is 1-7 cm at individual stations, with an average of 3.3cm (75% of their maximum amplitudes). The magnitudes of temporal changes in the regional averages of  $A_{sa}$  are much smaller than those of  $A_a$ . The consistency of the inter-annual variability of  $A_{sa}$  between different sub-regions is only found in the North East of Japan and the Sea of Japan.

#### 4. Forcing of the seasonal sea level cycle

##### 4.1 The IB effect and the steric height

###### *The IB effect ( $\eta_{IB}$ )*

The mean seasonal sea level cycle of  $\eta_{IB}$  over 1993-2013 is mapped in **Figure 6**.  $\eta_{IB}$  produces a significant annual sea level cycle over the whole area of study, except in small areas in the Sea of Okhotsk and the central middle-latitude (30-40°N) of Pacific. The annual cycle of  $\eta_{IB}$  exhibits the largest  $A_a$  ( $\sim 12$ cm) in the middle of the continental shelf, i.e. the north of the East China Sea (**Figure 6a**).  $\eta_{IB}$  has a uniform  $\phi_a$  (July) over most areas, except in the north central Pacific (35-60°N) where  $A_a$  is small and where  $\phi_a$  varies by  $\sim 6$  months (**Figure 6b**). The origin of the annual cycle of  $\eta_{IB}$  is linked with the strong seasonal variations of the air pressure at high latitudes due to the radiational heating [Yashayaev and Zveryaev, 2001; Gabler et al., 2008].

443 The atmospherically-induced semi-annual sea level cycle is only distinguishable  
 444 at the mid-latitudes (30-50°N) of the north Pacific and the west of the South  
 445 China Sea (**Figure 6c**). The maximum  $A_{sa}$  of ~3cm are located at the center of  
 446 middle-to-high latitudes (around 43°N and 170°E), but the values are less than  
 447 1cm in most marginal seas.  $\phi_{sa}$  is always in January or July, except in the Gulf of  
 448 Thailand (**Figure 6d**).

449 The inter-annual variability of the seasonal sea level cycle due to  $\eta_{IB}$  over the  
 450 same periods of tide gauge records was also calculated by using the long-term  
 451 atmospheric pressure data. Compared to  $\eta$ ,  $\eta_{IB}$  for tide gauge records has very  
 452 limited inter-annual variability (less than 3cm) both in  $A_a$  and in  $A_{sa}$ . The ranges  
 453 between maximum and minimum  $A_a$  of  $\eta_{IB}$  at individual stations over time are  
 454 up to 2.4cm in the north of the East China Sea (station number: 48) and 2.7cm in  
 455 the Sea of Okhotsk (station number: 120). The weak impact of  $\eta_{IB}$  on the long-  
 456 term changes of the seasonal sea level cycle is also revealed in the regional  
 457 averages (see the supplementary material **Figure S6**).

#### 458 ***The Steric height ( $\eta_{ster}$ )***

459 The mean seasonal cycle of  $\eta_{ster}$  derived from EN4 over 1993-2013 is shown in  
 460 **Figure 7**. The annual cycle of  $\eta_{ster}$  is significant in the whole area of study, with  
 461 larger  $A_a$  at the mid-latitudes and along the Kuroshio Current. The strongest  
 462 signal with  $A_a$  of 12-14cm is found in the East China Sea, the east of the Sea of  
 463 Japan and the east of Japan.  $\phi_a$  keeps homogeneous (~September) in the north  
 464 but it gradually shifts to January near the equator. The annual cycle in  $\eta_{ster}$  is  
 465 primarily determined by  $\eta_{thermo}$ .  $A_a$  of  $\eta_{halo}$  was found to be usually less than

466 1cm (not shown here). This is in agreement with the results by *Vinogradov et al.*  
467 [2008].

468 The semi-annual cycle of  $\eta_{ster}$  is statistically significant in the tropics and the  
469 north marginal seas (**Figure 7c**). The largest  $A_{sa}$  of 3cm is found in the east of  
470 Philippines and around the north of Japan.  $\phi_{sa}$  shifts quickly with different areas  
471 (**Figure 7d**). The semi-annual cycle in  $\eta_{ster}$  is also mainly caused by  $\eta_{thermo}$ .

472 The inter-annual variability of the seasonal cycle in  $\eta_{ster}$  at locations at least  
473 500m deep and closest to tide gauges was also estimated. The ranges of temporal  
474 changes of  $A_a$  and  $A_{sa}$  in  $\eta_{ster}$  are close to those as observed in  $\eta$ . However, there  
475 are only 32 (24) of the 120 stations where the inter-annual variability of  $A_a$   
476 ( $A_{sa}$ ) between  $\eta_{ster}$  and  $\eta$  is significantly correlated (at 95% confidence level).  
477 There is no change for the correlations when  $\eta_{IB}$  is removed from the observed  $\eta$   
478 (i.e.  $\eta - \eta_{IB}$ ), confirming the conclusion drawn above that  $\eta_{IB}$  has very limited  
479 influence on the long-term variability of the seasonal sea level cycle. The un-  
480 robust relationship between  $\eta$  and  $\eta_{ster}$  for their seasonal cycles can also be  
481 evidenced by the mismatching of their regional averages (see the supplementary  
482 material **Figure S6**). Significant correlations for the regional averages only exist  
483 for  $A_a$  over 1960-2013 in the east of the South China Sea, the East China Sea and  
484 the southeast of Japan ( $R=0.69, 0.39$  and  $0.29$  respectively).

485 When  $\eta - \eta_{IB}$  and  $\eta_{ster}$  from SODA during 1900-2010 are being used, the inter-  
486 annual variability of the seasonal amplitudes between the two sea level  
487 components is significantly correlated in most areas, except in the Sea of  
488 Okhotsk.  $\eta_{ster}$  explains more than 80% of inter-annual variations of  $A_a$  in  $\eta - \eta_{IB}$   
489 in the open ocean and the central South China Sea (**Figure 8**). At the coastal

regions, the relationships between  $\eta_{ster}$  and  $\eta - \eta_{IB}$  at seasonal scales become weak but still significant (at 95% confidence level), where  $\eta_{ster}$  explains 5-30% of inter-annual variability of  $A_a$  in  $\eta - \eta_{IB}$ . The relationships at the coastal regions are different from the un-robust correlations recognized between the tide gauge records and EN4 data (above paragraph). This inconsistency can be partly attributed to the fact that EN4 is an interpolated product which means that the steric values at a single point over the slope are the result of integrating observations from the shelf as well as from the open ocean. This is not the case in an ocean model, in which every single point is representative of the variability on its own location. On top of this, the length of tide gauge records may also have an impact, as they are always shorter than the SODA re-analysis (111years). Furthermore, it is also possible that SODA misses some processes that are recorded by tide gauges. What we can confirm at this moment from the two different assessments is that the contribution of  $\eta_{ster}$  to the inter-annual variations of the seasonal sea level cycle along the coasts is not as robust as that in the open ocean.

## 506 ***Residuals***

Removing  $\eta_{IB}$  and  $\eta_{ster}$  from the observed  $\eta$  permits the sea level residuals,  $\eta - \eta_{IB} - \eta_{ster}$ , which have significantly reduced  $A_a$  in the East China Sea, the Sea of Japan, the Luzon Strait and the open ocean, and at 89 of the 120 tide gauge records (**Figure 9a**). We recall here that  $\eta_{ster}$  is appointed as the values at the closest grid points over the continental slope (500 m deep). However, the annual cycle of  $\eta - \eta_{IB} - \eta_{ster}$  remains significant in most marginal seas and at 114 of the 120 tide gauge records.  $A_a$  with values of 5-10cm are found in the East China

514 Sea, the Sea of Okhotsk and spots of the Kuroshio Extension region. It is worth  
 515 noting that the removal of  $\eta_{IB}$  and  $\eta_{ster}$  increases  $A_a$  by 5-10cm in the west of  
 516 the South China Sea. This confirms the finding by *Ponte* [2006] that  $\eta_{IB}$  has a  
 517 negative contribution to the monthly sea level variance in the Southeast Asia.  $\phi_a$   
 518 of  $\eta - \eta_{IB} - \eta_{ster}$  varies gradually in each marginal sea, but more heterogeneous  
 519 features are found in the open ocean where  $A_a$  is low (**Figure 9b**).

520 The semi-annual cycle of  $\eta - \eta_{IB} - \eta_{ster}$  is still significant at 98 tide gauge  
 521 stations and in most areas of marginal seas (**Figure 9c-d**). Removal of  $\eta_{IB}$  and  
 522  $\eta_{ster}$  has limited influence on the semi-annual cycle in the marginal seas, except  
 523 in the Sea of Japan and the east of the Sea of Okhotsk. In these two areas,  $A_{sa}$   
 524 increases by 2-4cm when the two effects are subtracted. The existence of the  
 525 seasonal cycle in  $\eta - \eta_{IB} - \eta_{ster}$  indicates other mechanisms, beside  $\eta_{IB}$  and  
 526  $\eta_{ster}$ , to force the seasonal sea level cycle (e.g. wind effects). Of course, we cannot  
 527 rule out the possibility that  $\eta - \eta_{IB} - \eta_{ster}$  estimated here might be influenced  
 528 by the limitations of the dataset EN4 that is used to determine  $\eta_{ster}$ .

## 529 **4.2 Impacts from the wind stress and the sea surface currents**

530 As mentioned above,  $\eta_{IB}$  and  $\eta_{ster}$  cannot fully explain the whole budgets of the  
 531 observed seasonal sea level cycle either in its mean values or its inter-annual  
 532 variability, especially in the marginal seas. Therefore, in this subsection we  
 533 explored the potential contributions of the wind stress and the sea surface  
 534 currents by correlating the long-term seasonal cycle amplitudes. The wind stress  
 535 is expected to alter sea level variations via the mechanisms of ocean  
 536 upwelling/downwelling in coastal regions and water piling at the equator, which

are caused by the alongshore winds and the trade winds respectively through the Ekman transport [Segar, 2007]. In the open ocean, the vertical Ekman pumping due to the wind stress curl is able to produce the sea level variations as well, especially for the steric component because of the thermocline changes. The geostrophic balance is responsible for the mechanisms behind the links between sea level and horizontal sea surface currents. We performed the analyses in the seasonal cycle of  $\eta - \eta_{IB}$  and  $\eta - \eta_{IB} - \eta_{ster}$ , to distinguish the impacts of the two contributors on different components of sea level. The inter-annual variability of  $A_a$  and  $A_{sa}$  for the wind stress and the sea surface currents with different directions over 1900-2010 was calculated as mentioned in subsection 2.5. Because AVISO records (21 years) are not long enough to fully resolve the decadal changes in the seasonal sea level cycle and SODA, on the other hand, is able to reasonably reproduce the seasonal sea level cycle (as indicated in subsection 2.4), we used the sea surface height  $\eta - \eta_{IB}$  from SODA over the period 1900-2010 in this subsection instead, along with the observed  $\eta - \eta_{IB}$  from tide gauges over the same period.

### 553 **Wind stress**

The best correlations of the inter-annual variability of  $A_a$  in  $\eta - \eta_{IB}$  with that in different directions of wind stress nearby (with 1° radius around the location of sea level data) over 1900-2010 are shown in **Figure 10a**. The correlation coefficient is significant (at 95% confidence level) at 90 of the 120 tide gauge records and in most areas of the marginal seas. High correlations ( $R=0.6-0.9$ ) are found in the tropics and in the west areas of marginal seas. The direction of wind stress that corresponds to the best correlations with sea level is provided in the

561 supplementary material (**Figure S7**). In the western areas of marginal seas the  
562 annual cycle of sea level is better correlated with the zonal wind stress, while in  
563 the north Japan and the open ocean it is better correlated with the meridional  
564 wind stress component.

565 The regional averages of the inter-annual variability of  $A_a$  for tide gauge records  
566 are well correlated with the corresponding quantity for the wind stress (**Figure**  
567 **11a**), with  $R=0.58, 0.48, 0.59, 0.33, 0.48$  and  $0.41$  over 1960-2010 for the 6 sub-  
568 regions from south to north respectively.  $A_a$  of sea level is changing by about 2  
569 cm for every  $10^{-2} \text{ N/m}^2$  of changes in  $A_a$  of the wind stress for the regional  
570 averages.

571 When  $\eta_{ster}$  is removed, the correlation of  $A_a$  between sea level and wind stress  
572 remains nearly unchanged in the shallow waters of most marginal seas (**Figure**  
573 **10b**), except in the west of the Sea of Japan. This means that the temporal  
574 variations of the annual sea level cycle is dominated by  $\eta - \eta_{IB} - \eta_{ster}$  and this  
575 component is well related to the local wind. This identification could be  
576 interpreted as the results of the coastal upwelling/downwelling or the wind-  
577 driven sea surface currents in the coastal areas. **Figure 10** also shows that when  
578  $\eta_{ster}$  is excluded the relationship of sea level with wind stress disappears in the  
579 central of the Sea of Japan, the central of the South China Sea and the tropics. The  
580 annual cycle in  $\eta_{ster}$  over these areas can then be interpreted as wind stress-  
581 dependent. This might be caused by the vertical Ekman pumping and the  
582 equatorial upwelling that are both closely associated with the wind stress and  
583 that are both significant for modulating the steric height.



584 The semi-annual sea level cycle has significant correlations with nearby wind  
585 stress at 99 of the 120 tide gauge records and in large areas of marginal seas as  
586 well (not shown here). The best agreements for  $A_{sa}$  between sea level  
587 observations and the wind stress are in the northeast coasts of Japan and the  
588 west coasts of the South China Sea (**Figure 11b**). Similarly as revealed in the  
589 annual sea level cycle, the subtraction of  $\eta_{ster}$  does not apparently change the  
590 correlations with the wind stress for  $A_{sa}$  in the marginal seas.

#### 591 ***Sea surface currents***

592 The best correlations of the inter-annual variability of  $A_a$  between  $\eta - \eta_{IB}$  and  
593 the sea surface currents nearby are presented in **Figure 12a**. The correlation is  
594 significant at 117 of the 120 tide gauge records and in most areas. The  
595 relationships are stronger than those with the wind stress in most areas. Higher  
596 correlations ( $R=0.7-0.95$ ) appear in the regions where the ocean currents are  
597 known to be strong, such as the Oyashio and Kuroshio Currents regions  
598 [*Hurlburt et al.*, 1996] and the Luzon Strait [*Xue et al.*, 2004]. The direction of the  
599 sea surface currents that is allocated to the best correlations with sea level varies  
600 regionally except in subtropical areas where the associations seem to be more  
601 determined by the meridional currents (**Figure S8** in supplementary). The fast  
602 changes of the surface current direction for the best correlations indicate that  
603 the geostrophic response of sea level might be acting locally and at small scales.  
604 Also, we are aware that our method may not work well if the current direction  
605 for the best correlations is changing in time. This limitation may cause fast  
606 changes in the identified direction of the surface currents as well.

607 The regional averages of  $A_a$  anomalies of sea level from tide gauge observations  
608 correlate well with the changes in the surface currents, with  $R=0.63, 0.45, 0.82,$   
609  $0.71, 0.69$  and  $0.62$  over 1960-2010 for the six sub-regions from south to north  
610 respectively (**Figure 13a**). The regression for  $A_a$  is approximately 2 cm of  
611 increase in sea level for 1 cm/s increase in the current speed. However, this scale  
612 is greatly reduced prior to 1960 when the surface currents have larger range of  
613 variations (**Figure 13a**). This is due to the fact that the magnitude of the  
614 geostrophic response of sea level to nearby surface currents varies with  
615 locations (see the supplementary material **Figure S9**) presumably because of  
616 topography changes and thus the calculation of regional averages using fewer  
617 individual records prior to 1960 (**Figure 1b**) leads to the average values that  
618 reflect more localized features rather than the regional average features.

619 When  $\eta_{ster}$  is excluded from  $\eta - \eta_{IB}$ ,  $A_a$  of sea level is still highly dependent on  
620 the surface currents at 117 of the 120 tide gauge records, in the shallow waters  
621 of marginal seas and in the north of the Oyashio Current region (**Figure 12b**).  
622 This indicates that in these areas  $\eta - \eta_{IB} - \eta_{ster}$  dominates the relationships of  
623  $\eta - \eta_{IB}$  with the surface currents due to the geostrophic balance as expected.  
624 This can be further evidenced by comparing the time series of  $A_a$  in  $\eta_{ster}$  and in  
625  $\eta - \eta_{IB} - \eta_{ster}$  with the corresponding quantity in the surface currents at  
626 specific points (**Figure 14a-b**). At location A [ $8^\circ\text{N}, 108^\circ\text{E}$ ] in the Gulf of Thailand,  
627 the inter-annual variability of  $A_a$  in  $\eta_{ster}$ , the dominating component in sea level,  
628 is significantly correlated with the variability of the local surface current  
629 ( $R=0.78$ ). In contrast, changes in  $\eta_{ster}$  have no links with the current ( $R=0.1$ , not  
630 significant at 95% confidence level). When location B [ $38^\circ\text{N}, 123^\circ\text{E}$ ] in the East

631 China Sea is selected,  $A_a$  in  $\eta_{ster}$  becomes comparable to that in  $\eta - \eta_{IB} - \eta_{ster}$ .  
632 The surface current has a significant correlation with  $\eta_{ster}$  ( $R=0.23$ ), but it has an  
633 even stronger correlation with  $\eta - \eta_{IB} - \eta_{ster}$  ( $R=0.45$ ).

634 However, the removal of  $\eta_{ster}$  eliminates the high correlations that are identified  
635 for sea level in the open oceans, particularly in the areas of the south Oyashio,  
636 the Kuroshio and the North Equatorial Currents, and in the Luzon Strait (**Figure**  
637 **12**). The disappearance of correlations in these areas implies that  $\eta_{ster}$ , as the  
638 dominating component of sea level in the open ocean, is firmly regulated by the  
639 surface currents. Time series of the variables at two locations in these areas are  
640 also plotted to support this argument (**Figure 14c-d**). At location C [ $37^\circ\text{N}$ ,  
641  $143^\circ\text{E}$ ] on the route of the Kuroshio Current, the temporal variations of  $A_a$   
642 between  $\eta_{ster}$  and the surface current are very well matched ( $R=0.90$ ). At  
643 location D [ $4^\circ\text{N}$ ,  $143^\circ\text{E}$ ] near to the North Equatorial Current, they are  
644 significantly correlated as well but with a reduced correlation coefficient  
645 ( $R=0.33$ ).

646 It is worth noticing that the surface currents and the wind stress used in the  
647 analysis cannot be independent. The inter-annual variability of their seasonal  
648 cycles shows significant correlations in the marginal seas (except in the Sea of  
649 Japan) and in the tropics, with  $R=0.7-0.95$  (see the supplementary material  
650 **Figure S10**). Thus, the relationships of sea level with the surface currents that  
651 are found in the marginal seas and in the tropics (**Figure 12**) could be thought to  
652 be the consequence of the impact from the local wind. However, no significant  
653 correlations between the surface currents and the wind stress are found in the  
654 open ocean, particularly in the regions with the strong currents, where no robust

655 correlations are found between sea level and the wind stress either (**Figure 10**).  
656 Therefore, the high correlations of sea level with the surface currents in these  
657 areas can be further interpreted as the consequence of the geostrophic balance  
658 between  $\eta_{ster}$  and the large-scale ocean currents, which are not forced by the  
659 local wind field.

660 The changes in  $A_{sa}$  of sea level are significantly correlated with the changes in  
661 the surface currents at 117 tide gauge records and in most areas (not shown  
662 here). The results for the regional averages of tide gauge records are shown in  
663 **Figure 13b**. The correlations are again better than those obtained from the wind  
664 stress.

665

## 666 **5. Conclusions**

667 The spatial and temporal features of the seasonal sea level variations in the  
668 northwest Pacific have been described by investigating the sea level  
669 observations from tide gauges (1900-2013) and gridded altimetry product  
670 AVISO (1993-2013). In the marginal seas, 60-95% of the monthly sea level  
671 variance can be explained by the annual and semi-annual cycles, except in the  
672 Sea of Okhotsk where the seasonal sea level variance is weak and sea ice  
673 becomes important [*Parkinson et al.*, 1999]. However, in the open ocean and  
674 especially in eddy-rich regions (e.g. the Kuroshio Extension and the Oyashio  
675 Current) where the monthly sea level is mainly driven by the mesoscale eddies,  
676 the regular seasonal oscillations only account for 3-20% of the observed sea  
677 level variance.

678 The annual sea level cycle is significant over the whole area of study, with  $A_a$   
 679 over 10cm in the East China Sea, the Luzon Strait, the Gulf of Thailand and the  
 680 Kuroshio Current regions. The largest  $A_a$  of  $\sim 30$  cm is observed in the north of  
 681 the East China Sea. The semi-annual sea level cycle is only significant along the  
 682 coasts and in the shallow waters of most marginal seas. The largest  $A_{sa}$  is  $\sim 6$ cm  
 683 on the northwestern coasts of the South China Sea. The seasonal cycle  
 684 parameters of sea level estimated from tide gauge records and AVISO were  
 685 compared. At the sites closest to tide gauge stations, AVISO significantly  
 686 underestimates  $A_a$  by 2-9cm (25%) at 59 of 120 stations and  $A_{sa}$  by 1-3 cm  
 687 (60%) at 28 stations. The discrepancies mainly occur on the coasts of China and  
 688 Russia.

689 The contributions of the IB effect ( $\eta_{IB}$ ) and the steric height ( $\eta_{ster}$ ) to the  
 690 observed seasonal sea level cycle have been identified.  $\eta_{IB}$  has significant impact  
 691 on the annual sea level cycle over the whole area of study, which causes the  
 692 largest  $A_a$  of 12cm in the East China Sea. The semi-annual cycle of  $\eta_{IB}$  is only  
 693 significant at the central north Pacific where  $A_{sa}$  is  $\sim 3$ cm.  $\eta_{ster}$ , mainly due to  
 694 the thermal expansion of seawater, can produce  $A_a$  with up to 8-12cm in the East  
 695 China Sea, the east of Sea of Japan and the Kuroshio Extension region. The  
 696 removal of  $\eta_{IB}$  and  $\eta_{ster}$  significantly diminishes the annual sea level cycle in  
 697 most areas, but increases the annual cycle by 5-10cm in the west of the South  
 698 China Sea. The removal has little impact on the semi-annual cycle. Significant  
 699 seasonal cycles still remain in the residuals over the marginal seas.

700 The long-term tide gauge observations allow us to assess the temporal  
 701 variability of the seasonal sea level variations on the coasts. The annual and

702 semi-annual sea level cycles are not stable with time, with amplitudes changing  
703 between 2-20.4cm and 1-7cm respectively.  $\eta_{IB}$  and  $\eta_{ster}$  have limited influences  
704 on the observed inter-annual variability of the seasonal sea level cycle based on  
705 our analysis. However, in the open ocean  $\eta_{ster}$  explains over 80% of inter-annual  
706 variations based on ocean reanalysis of SODA.

707 The dynamic forcing of the inter-annual variability in the seasonal sea level cycle  
708 was also diagnosed using SODA data. The wind stress and especially the sea  
709 surface currents are correlated with the seasonal sea level cycle at most tide  
710 gauge records and in the marginal seas, as the consequence of their strong  
711 contributions to the sea level residuals. The regional averages of the seasonal  
712 cycle amplitudes are changing by  $\sim 2\text{cm}$  for  $10^{-2} \text{ N/m}^2$  and  $1 \text{ cm/s}$  changes in the  
713 amplitudes of the wind stress and the surface currents respectively. Because in  
714 the marginal seas and in the tropics the seasonal variations of the currents are  
715 highly dependent on the local wind stress, the relationships of sea level with the  
716 surface currents observed here can be interpreted as the consequence of the  
717 wind-driven Ekman transport. In the open ocean, especially in the regions of the  
718 western boundary currents, the surface currents can better describe the  
719 seasonal sea level variations ( $R=0.7-0.95$ ) than the wind stress, and this is mainly  
720 due to the significant associations between the steric height and the open ocean  
721 currents through the geostrophic equilibrium. However, there are still some  
722 areas in the open ocean, where neither the wind stress nor the surface currents  
723 can well explain the forcing of the seasonal steric height variations which  
724 account for over 80% of sea level changes. The vertical Ekman pumping caused

725 by the wind stress curl might be the reason and we will work on this in the  
726 future.

727

## 728 **Acknowledgements**

729 This research is funded by Lloyd's Register Foundation, which supports the  
730 advancement of engineering-related education, and funds research and  
731 development that enhances safety of life at sea, on land and in the air. X. Feng  
732 and J. Zheng appreciate the National Science Fund for Distinguished Young  
733 Scholars (Grant No.51425901). G. Jordà and M. Marcos acknowledge two Ramón  
734 y Cajal contracts funded by the Spanish Ministry of Economy and the Regional  
735 Government of the Balearic Islands. Tide gauge data used in the paper were  
736 obtained from the Permanent Service for Mean Sea Level ([www.psmsl.org](http://www.psmsl.org)), and  
737 gridded satellite altimeter sea level records and DAC data were retrieved from  
738 AVISO ([www.aviso.altimetry.fr](http://www.aviso.altimetry.fr)). The ocean objective analyses EN4.0.2 were  
739 collected from the UK Met Office Hadley Centre  
740 ([www.metoffice.gov.uk/hadobs/en4](http://www.metoffice.gov.uk/hadobs/en4)), and the wind stress, the sea surface  
741 currents and the reanalysis of other oceanic data were collected from SODA  
742 developed by Texas A&M University (<http://soda.tamu.edu>). The sea level  
743 pressure was retrieved from the NOAA's 20<sup>th</sup> century reanalysis and the  
744 ECMWF-Interim. We thank all these institutions for making their data publically  
745 available, as well as three reviewers for their constructive comments and  
746 suggestions.

747

748 **Reference**

- 749 Amiruddin, A. M., I. D. Haigh, M. N. Tsimplis, F. M. Calafat, and S. Dangendorf (2015), The seasonal  
750 cycle and variability of sea level in the South China Sea, *Journal of Geophysical Research:*  
751 *Oceans*, 120, doi:10.1002/2015JC010923
- 752 Anderson, C. J. and Lockaby, B. G. (2012), Seasonal patterns of river connectivity and saltwater  
753 intrusion in tidal freshwater forested wetlands, *River Research and Applications*, 28, 814–826,  
754 doi: 10.1002/rra.1489
- 755 Barbosa, S.M., M.E Silva, and M.J. Fernandes (2008), Changing seasonality in North Atlantic coastal  
756 sea level from the analysis of long tide gauge records, *Tellus A*, 60: 165–177, doi:  
757 10.1111/j.1600-0870.2007.00280.x
- 758 Bingham, R. J., and C. W. Hughes (2012), Local diagnostics to estimate density-induced sea level  
759 variations over topography and along coastlines, *Journal of Geophysical Research: Oceans*, 117,  
760 C01013, doi:10.1029/2011JC007276.
- 761 Boyer, T. P., et al. (2009), World Ocean Database 2009, edited S. Levitus, 216 pp., NOAA Atlas  
762 NESDIS 66, U.S. Gov. Print. Off., Washington, D. C.
- 763 Carrère, L., and F. Lyard (2003), Modeling the barotropic response of the global ocean to atmospheric  
764 wind and pressure forcing - comparisons with observations, *Geophysical Research Letters*, 30(6),  
765 1275, doi:10.1029/2002GL016473.
- 766 Carton, J. A., and B. S. Giese (2008), A reanalysis of ocean climate using Simple Ocean Data  
767 Assimilation (SODA), *Monthly Weather Review*, 136(8), 2999-3017,  
768 doi:10.1175/2007MWR1978.1.
- 769 Carton, J. A., G., Chepurin, X., Cao, and B., Giese (2000), A simple ocean data assimilation analysis of  
770 the global upper ocean 1950-95. Part I: Methodology, *Journal of Physical Oceanography*, 30(2),  
771 294-309, doi:10.1175/1520-0485(2000)030<0294:ASODAA>2.0.CO;2.
- 772 Chelton, D. B., M. G. Schlax, and R. M. Samelson (2011), Global observations of nonlinear mesoscale  
773 eddies, *Progress in Oceanography*, 91, 167-216.
- 774 Chen, J. L., C. K. Shum, C. R. Wilson, D. P. Chambers, and B. D. Tapley (2000), Seasonal sea level  
775 change from TOPEX/Poseidon observation and thermal contribution, *Journal of Geodesy*,  
776 73(12), 638-647, doi:10.1007/s001900050002.
- 777 Compo, G., et al. (2011), The twentieth century reanalysis project, *Quarterly Journal of the Royal*  
778 *Meteorological Society*, 137(654), 1–28, doi:10.1002/qj.776.



779 Dangendorf, S., C. Mudersbach, J. Jensen, G. Anette, and H. Heinrich (2013a), Seasonal to decadal  
780 forcing of high water level percentiles in the German Bight throughout the last century, *Ocean*  
781 *Dynamics*, 63(5), 533-548, doi: 10.1007/s10236-013-0614-4

782 Dangendorf, S., T. Wahl, C. Mudersbach, and J. Jensen (2013b), The Seasonal mean sea level cycle in  
783 the Southeastern North Sea, *Journal of Coastal Research*, Special Issue No. 65, pp. 1915-1920,  
784 ISSN 0749-0208

785 Feng, X., and M. N. Tsimplis (2014), Sea level extremes at the coasts of China, *Journal of Geophysical*  
786 *Research: Oceans*, 119, 1593–1608, doi:10.1002/2013JC009607.

787 Feng, X., M. N. Tsimplis, and P. L. Woodworth (2015), Nodal variations and long-term changes in the  
788 main tides on the coasts of China, *Journal of Geophysical Research: Oceans*, 120, 1215–1232,  
789 doi:10.1002/2014JC010312.

790 Gabler, R., J., Petersen, L., Trapasso, and D., Sack (2008), Physical geography (ninth edition),  
791 Cengage Learning, 672pp.

792 Giese, B. S. and S. Ray (2011), El Niño variability in simple ocean data assimilation (SODA), 1871–  
793 2008, *J. Geophys. Res.*, 116, C02024, doi:10.1029/2010JC006695.

794 Gill, A. E. (1982), Atmosphere-ocean dynamics (Vol. 30). Academic press.

795 Good, S. A., M. J. Martin, and N. A. Rayner (2013), EN4: Quality controlled ocean temperature and  
796 salinity profiles and monthly objective analyses with uncertainty estimates, *Journal of*  
797 *Geophysical Research: Oceans*, 118, 6704–6716, doi:10.1002/2013JC009067.

798 Haines, K., M. Valdivieso, H. Zuo, and V. N. Stepanov (2012), Transports and budgets in a 1/4 °  
799 global ocean reanalysis 1989–2010, *Ocean Science*, 8, 333-344, doi:10.5194/os-8-333-2012

800 Hamlington, B.D., R.R. Leben, R.S. Nerem, and K.-Y. Kim (2010), New method for reconstructing sea  
801 level from tide gauges using satellite altimetry, Geoscience and Remote Sensing Symposium  
802 (IGARSS), 2010 IEEE International, pp.781-784, doi: 10.1109/IGARSS.2010.5651050

803 Hamlington, B. D., R. R. Leben, R. S. Nerem, W. Han, and K.-Y. Kim (2011), Reconstructing sea level  
804 using cyclostationary empirical orthogonal functions, *Journal of Geophysical Research: Oceans*,  
805 116, C12015, doi:10.1029/2011JC007529

806 Hamlington, B. D., R. R. Leben, L. A. Wright, and K.-Y. Kim (2012), Regional sea level  
807 reconstruction in the Pacific ocean. *Marine Geodesy*, 35(sup1), 98-117, doi:  
808 10.1080/01490419.2012.718210

809 Han, G., and W., Huang (2008), Pacific decadal oscillation and sea level variability in the Bohai,  
810 Yellow, and East China seas, *Journal of Physical Oceanography*, 38(12), 2772-2783, doi:  
811 10.1175/2008JPO3885.1.

812 Holgate, S. J., et al. (2012), New data systems and products at the permanent service for mean sea  
813 level, *Journal of Coastal Research*, 29(3), 493-504, doi:10.2112/JCOASTRES-D-12-00175.1.

814 Hünicke, B., and E., Zorita (2008), Trends in the amplitude of Baltic Sea level annual cycle, *Tellus A*,  
815 60: 154-164, doi: 10.1111/j.1600-0870.2007.00277.x

816 Hurlburt, H. E., A. J. Wallcraft, W. J. Schmitz Jr., P. J. Hogan, and E. J. Metzger (1996), Dynamics of  
817 the Kuroshio/Oyashio current system using eddy-resolving models of the North Pacific Ocean,  
818 *Journal of Geophysical Research: Oceans*, 101(C1), 941–976, doi:10.1029/95JC01674.

819 Kang, S. K., M. G. G. Foreman, H.-J. Lie, J.-H. Lee, J. Cherniawsky, and K.-D. Yum (2002), Two-  
820 layer tidal modeling of the Yellow and East China Seas with application to seasonal variability of  
821 the M<sub>2</sub> tide, *Journal of Geophysical Research: Oceans*, 107(C3), doi:10.1029/2001JC000838.

822 Marcos, M., and M. N. Tsimplis (2007), Variations of the seasonal sea level cycle in southern Europe,  
823 *Journal of Geophysical Research: Oceans*, 112, C12011, doi:10.1029/2006JC004049.

824 Marcos, M., M. N. Tsimplis, and F. M. Calafat (2012), Inter-annual and decadal sea level variations in  
825 the north-western Pacific marginal seas, *Progress in Oceanography*, 105, 4-21,  
826 doi:10.1016/j.pocean.2012.04.010.

827 Müller, M., J. Cherniawsky, M. Foreman, and J.-S. von Storch (2014), Seasonal variation of the M<sub>2</sub>  
828 tide, *Ocean Dynamics* 64(2), 159-177, doi:10.1007/s10236-013-0679-0.

829 Parkinson, C. L., D. J. Cavalieri, P. Gloersen, H. J. Zwally, and J. C. Comiso (1999), Arctic sea ice  
830 extents, areas, and trends, 1978–1996, *Journal of Geophysical Research: Oceans*, 104(C9),  
831 20837-20856, doi:10.1029/1999JC900082.

832 Pascual, A., M. Marcos, and D. Gomis (2008), Comparing the sea level response to pressure and wind  
833 forcing of two barotropic models: Validation with tide gauge and altimetry data, *Journal of*  
834 *Geophysical Research: Oceans*, 113, C07011, doi:10.1029/2007JC004459.

835 Passaro, M., P. Cipollini, and J. Benveniste (2015), Annual sea level variability of the coastal ocean:  
836 The Baltic Sea-North Sea transition zone, *Journal of Geophysical Research: Oceans*, 120, 3061–  
837 3078, doi:10.1002/2014JC010510.

838 Plag, H.-P., and M.N., Tsimplis (1999), Temporal variability of the seasonal sea-level cycle in the  
839 North Sea and Baltic Sea in relation to climate variability, *Global and Planetary Change*, 20,  
840 173-203, doi:10.1016/S0921-8181(98)00069-1

841 Ponte, R. M. (2006), Low-frequency sea level variability and the inverted barometer effect, *Journal of*  
842 *Atmospheric and Oceanic Technology*, 23(4), 619-629, doi: 10.1175/JTECH1864.1.

843 Pugh, D. and P. Woodworth (2014), Sea-level science: understanding tides, surges, tsunamis and mean  
844 sea-level changes , Cambridge University Press , UK 395 pp.

845 Segar, D.A. (2007), Introduction to Ocean Sciences, W. W. Norton and Company, Inc., New York,  
846 U.S.A. 720pp.

847 Smith, R. D., J. K., Dukowicz, and R. C., Malone (1992), Parallel ocean general circulation modeling,  
848 *Physica D: Nonlinear Phenomena*, 60(1), 38-61, doi: 10.1016/0167-2789(92)90225-C.

849 Tabata, S., B., Thomas, and D., Ramsden (1986), Annual and interannual variability of steric sea level  
850 along line P in the northeast Pacific Ocean, *Journal of Physical Oceanography*, 16(8), 1378-  
851 1398. doi: 10.1175/1520-0485(1986)016<1378:AAIVOS>2.0.CO;2.

852 Tamisiea, M. E., E. M. Hill, R. M. Ponte, J. L. Davis, I. Velicogna, and N. T. Vinogradova (2010),  
853 Impact of self-attraction and loading on the annual cycle in sea level, *Journal of Geophysical*  
854 *Research-Oceans*, 115, C07004, doi:10.1029/2009JC005687

855 Torres, R. R., and M. N. Tsimplis (2012), Seasonal sea level cycle in the Caribbean Sea, *Journal of*  
856 *Geophysical Research: Oceans*, 117, C07011, doi:10.1029/2012JC008159.

857 Tsimplis, M. N., and P. L. Woodworth (1994), The global distribution of the seasonal sea level cycle  
858 calculated from coastal tide gauge data, *Journal of Geophysical Research*, 99(C8), 16031–16039,  
859 doi:10.1029/94JC01115.

860 Tsimplis, M. N. and A. G. P. Shaw (2010), Seasonal sea level extremes in the Mediterranean Sea and  
861 at the Atlantic European coasts, *Natural Hazards and Earth System Sciences*, 10, 1457-1475,  
862 doi:10.5194/nhess-10-1457-2010

863 UNESCO (1981), Tenth Report of the International oceanographic Tables. UNESCO Technical Papers  
864 in Marine Science 36, 25.

865 Vignudelli S., Kostianoy A. G., Cipollini P., Benveniste J. (Editors) (2011), Coastal Altimetry,  
866 Springer-Verlag Berlin Heidelberg, 578 pp, doi:10.1007/978-3-642-12796-0.

867 Vinogradov, S. V., and R. M. Ponte (2010), Annual cycle in coastal sea level from tide gauges and  
868 altimetry, *Journal of Geophysical Research: Oceans*, 115, C04021, doi:10.1029/2009JC005767.

869 Vinogradov, S. V., R. M. Ponte, P. Heimbach, and C. Wunsch (2008), The mean seasonal cycle in sea  
870 level estimated from a data-constrained general circulation model, *Journal of Geophysical*  
871 *Research: Oceans*, 113, C03032, doi:10.1029/2007JC004496.

872 Wahl, T., F. M. Calafat, and M. E. Luther (2014), Rapid changes in the seasonal sea level cycle along  
873 the US Gulf coast from the late 20th century, *Geophysical Research Letters*, 41, 491–498,  
874 doi:10.1002/2013GL058777.

875 Woodruff, S. D., et al. (2011), ICOADS Release 2.5: extensions and enhancements to the surface  
876 marine meteorological archive, *International Journal of Climatology*, 31: 951–967. doi:  
877 10.1002/joc.2103.

878 Wunsch, C., and D. Stammer (1997), Atmospheric loading and the oceanic “inverted barometer”  
879 effect, *Reviews of Geophysics*, 35(1), 79–107, doi:10.1029/96RG03037.

880 Xue, H., F. Chai, N. Pettigrew, D. Xu, M. Shi, and J. Xu (2004), Kuroshio intrusion and the circulation  
881 in the South China Sea, *Journal of Geophysical Research*, 109, C02017,  
882 doi:10.1029/2002JC001724.

883 Yashayaev, I. M. and Zveryaev, I. I. (2001), Climate of the seasonal cycle in the North Pacific and the  
884 North Atlantic oceans. *International Journal of Climatology*, 21: 401–417. doi:10.1002/joc.585.

885 Wang, W., H. Liu, Y. Li, and J. Su (2014), Development and management of land reclamation in  
886 China, *Ocean and Coastal Management*, 102, 415-425. doi:10.1016/j.ocecoaman.2014.03.009.

887

888

**Figure 1.**  
Study areas and locations of 120 tide gauges (**a**), and periods of valid  $\eta$  observed from tide gauges (**b**). Tide gauges are colored and numbered into six sub-regions, with five stations treated as outliers (black dots). The six sub-regions are named as the east of the South China Sea (SCS-E), the west of the South China Sea (SCS-W), the East China Sea (ECS), the Sea of Japan (SoJ), the northeast coasts of Japan (Japan-NE) and the southeast coasts of Japan (Japan-SE). KS, LS and GTL represent the Korea Strait, the Luzon Strait and the Gulf of Thailand respectively.

**Figure 2.**  
Variance of  $\eta$  observed from tide gauges and AVISO (**a**), and percentage of the variance explained by the seasonal cycle (**b**). Schematic routes of the Oyashio, the Kuroshio and the North Equatorial Currents are indicated by the black dashed lines in (**a**), which are estimated using the altimeter data distributed by AVISO.

**Figure 3.**  
Mean  $A_a$  (**a**),  $\phi_a$  (**b**),  $A_{sa}$  (**c**) and  $\phi_{sa}$  (**d**) of  $\eta$  from tide gauges and AVISO. Blank areas and circles indicate the estimates of the annual or semi-annual cycle parameters that are not passing the significance test at 95% confidence level.

**Figure 4.**  
Differences of mean  $A_a$  (**a**),  $\phi_a$  (**b**),  $A_{sa}$  (**c**) and  $\phi_{sa}$  (**d**) of  $\eta$  determined by tide gauges and AVISO at the closest points to tide gauges (TG) (AVISO – tide gauges). Black bars indicate the differences that pass the significance test, i.e. error bars of two estimated values (one from AVISO and the other from tide gauges) used in comparison do not overlap, while grey bars indicate the insignificant differences.

**Figure 5.**  
Time series of the anomaly of  $A_a$  (**a**) and  $A_{sa}$  (**b**) of  $\eta$  determined from tide gauges, which are grouped by 6 sub-regions as specified in **Figure 1**. Bold black line is plotted for the regional ensemble average of individual anomalies in each sub-region.

**Figure 6.**  
Mean  $A_a$  (**a**),  $\phi_a$  (**b**),  $A_{sa}$  (**c**) and  $\phi_{sa}$  (**d**) for  $\eta_{IB}$  derived from DAC data over 1993-2013. Blank areas indicate the estimates of the annual or semi-annual cycle parameters that are not passing the significance test at 95% confidence level. Please note that the scales of amplitudes here are different from those in **Figure 3**.

**Figure 7.**  
Mean  $A_a$  (**a**),  $\phi_a$  (**b**),  $A_{sa}$  (**c**) and  $\phi_{sa}$  (**d**) for  $\eta_{ster}$  derived from EN4 over 1993-2013. Blank areas indicate the estimates of the annual or semi-annual cycle parameters that are not passing the significance test at 95% confidence level. Please note that the scales of amplitudes here are different from those in **Figure 3**.

**Figure 8.**  
Percentage of the inter-annual variability of  $A_a$  (**a**) and  $A_{sa}$  (**b**) for  $\eta - \eta_{IB}$  explained by that of  $\eta_{ster}$  over 1900-2010, derived from SODA. Blank areas indicate the grids where the correlation of the inter-annual variability of  $A_a$  or  $A_{sa}$  between  $\eta - \eta_{IB}$  and  $\eta_{ster}$  are not significant at 95% confidence level.

**Figure 9.**  
Mean  $A_a$  (**a**),  $\phi_a$  (**b**),  $A_{sa}$  (**c**) and  $\phi_{sa}$  (**d**) for  $\eta - \eta_{IB} - \eta_{ster}$  when  $\eta_{IB}$  and  $\eta_{ster}$  are removed from  $\eta$  provided by tide gauges and AVISO. Blank circles and areas indicate the estimates of the annual or semi-annual cycle parameters that are not passing the significance test at 95% confidence level.

**Figure 10.**  
**(a)** Best correlation coefficients of the inter-annual variability of  $A_a$  between  $\eta - \eta_{IB}$ , provided by tide gauges and SODA, and the nearby wind stress; **(b)** same as **(a)**, but for the correlations between  $\eta - \eta_{IB} - \eta_{ster}$  and the nearby wind stress. Blank circles and areas indicate the correlations that do not pass the significance test at 95% confidence level. Note that the direction of wind stress corresponding to the best correlation coefficients is provided in the supplementary material **Figure S7**.

**Figure 11.**  
Time series of regional average anomaly of  $A_a$  (**a**) and  $A_{sa}$  (**b**) for  $\eta - \eta_{IB}$  (black) against the corresponding average of the wind stress (red) in 6 sub-regions as specified in **Figure 1**.

**Figure 12.**  
Same as **Error! Reference source not found.**, but for best correlations with the nearby sea surface currents. Black dots in **(a)** highlight 4 grid points: A [8°N, 108°E], B [38°N, 123°E], C [37°N, 143°E] and D [4°N, 143°E]. Note that the direction of surface currents corresponding to the best correlation coefficients with sea level is provided in the supplementary material **Figure S8**.

**Figure 13.**  
Same as **Figure 11**, but for time series of the sea surface currents (red).

**Figure 14.**  
Time series of  $A_a$  for  $\eta - \eta_{IB} - \eta_{ster}$  (green) and  $\eta_{ster}$  (red), along with the corresponding quantity of the sea surface currents that are best corrected with time series for  $\eta - \eta_{IB}$ , at 4 grid points A-D (**a-d**) as indicated in **Error! Reference source not found.a**.

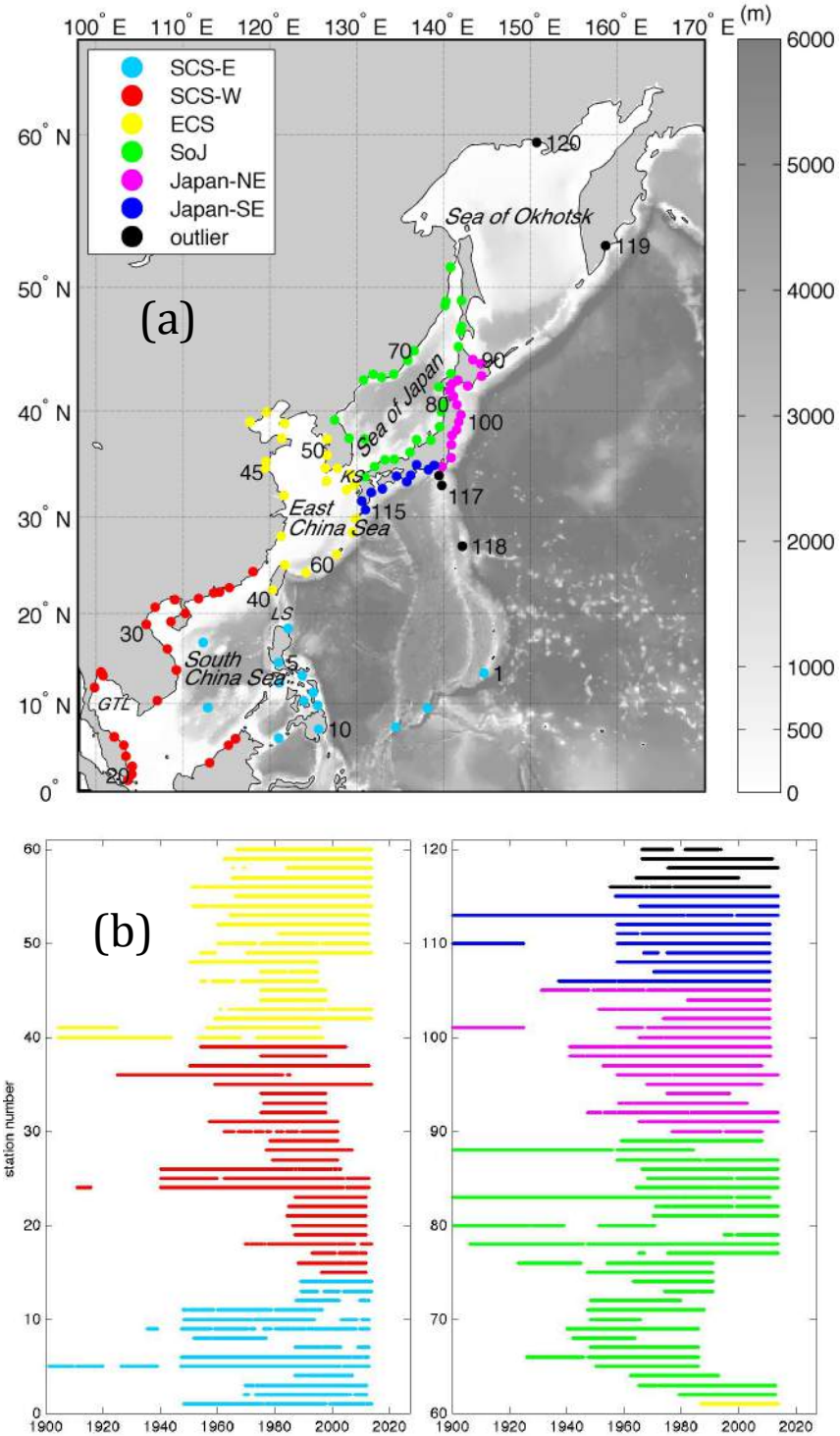


**Figure 1.** Study areas and locations of 120 tide gauges (a), and periods of valid  $\eta$  observed from tide gauges (b). Tide gauges are colored and numbered into six sub-regions, with five stations treated as outliers (black dots). The six sub-regions are named as the east of the South China Sea (SCS-E), the west of the South China Sea (SCS-W), the East China Sea (ECS), the Sea of Japan (SoJ), the northeast coasts of Japan (Japan-NE) and the southeast coasts of Japan (Japan-SE). KS, LS and GTL represent the Korea Strait, the Luzon Strait and the Gulf of Thailand respectively.

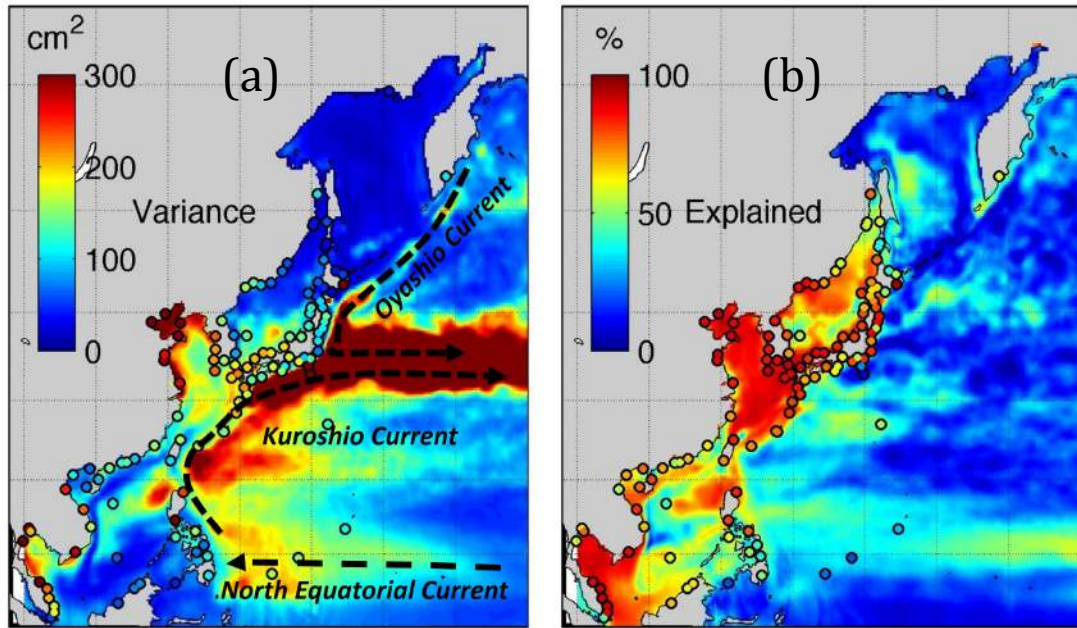


**Figure 2.** Variance of  $\eta$  observed from tide gauges and AVISO (a), and percentage of the variance explained by the seasonal cycle (b). Schematic routes of the Oyashio, the Kuroshio and the North Equatorial Currents are indicated by the black dashed lines in (a), which are estimated using the altimeter data distributed by AVISO.



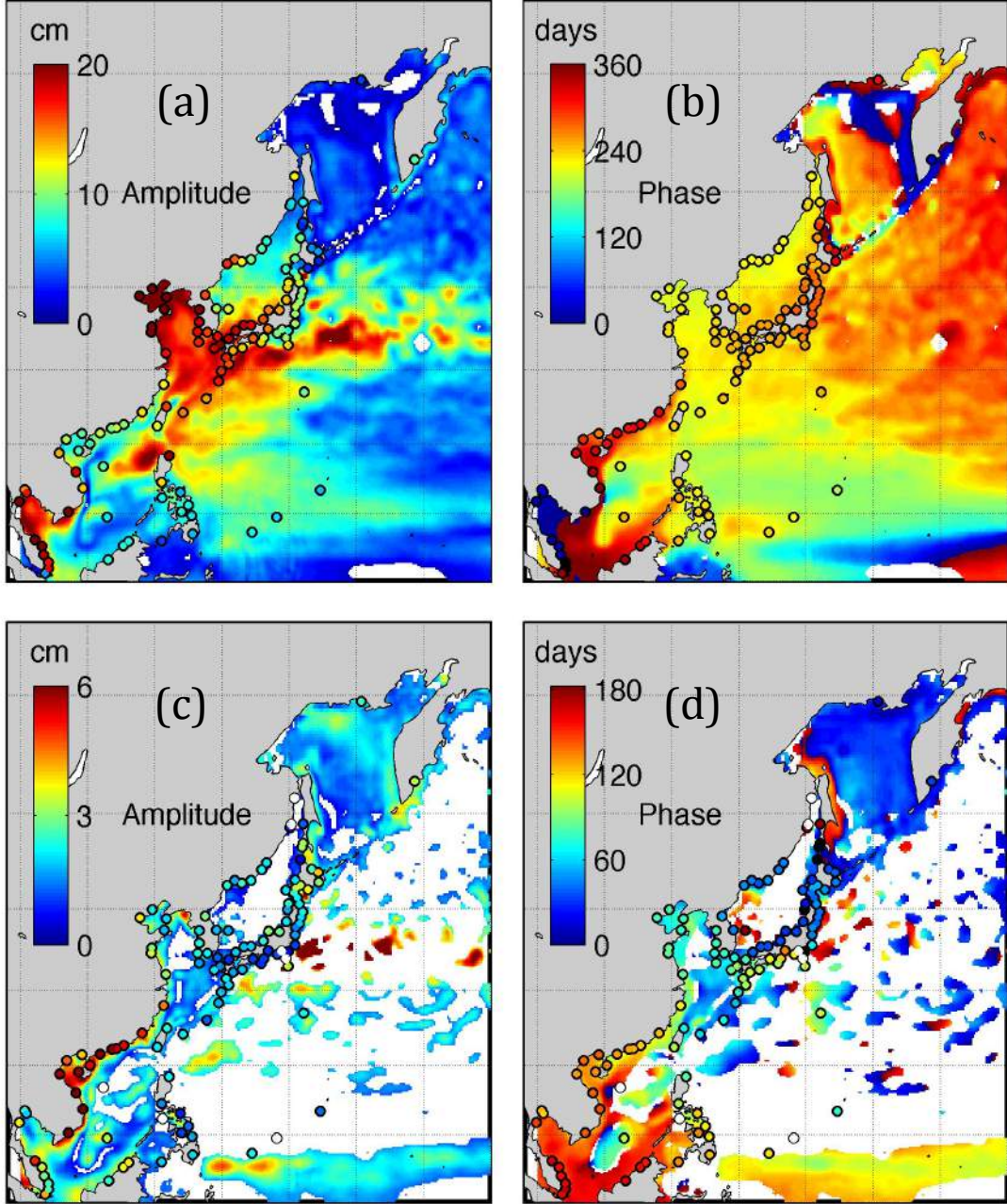


**Figure 3.** Mean  $A_a$  (a),  $\phi_a$  (b),  $A_{sa}$  (c) and  $\phi_{sa}$  (d) of  $\eta$  from tide gauges and AVISO. Blank areas and circles indicate the estimates of the annual or semi-annual cycle parameters that are not passing the significance test at 95% confidence level.

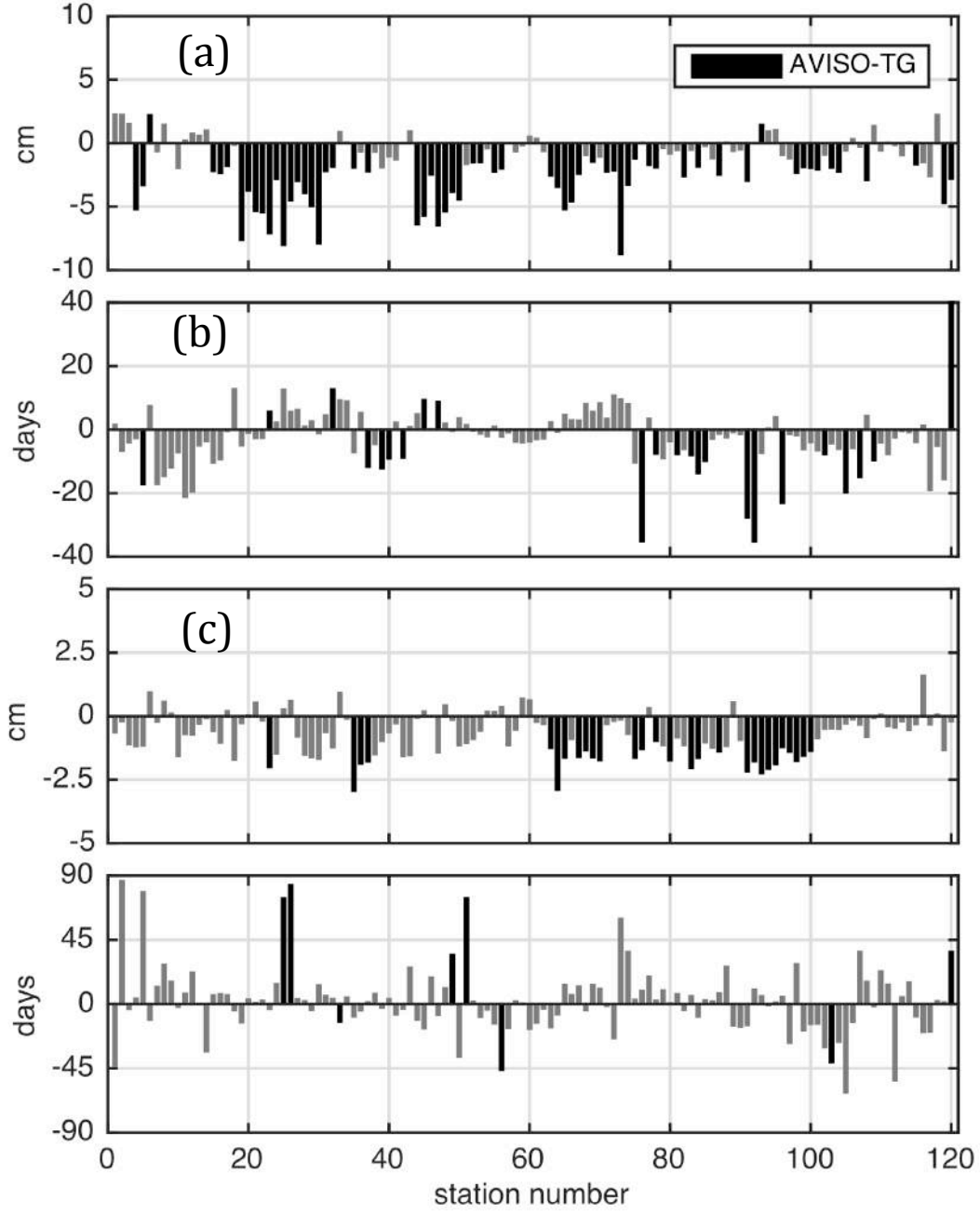


**Figure 4.** Differences of mean  $A_a$  (a),  $\phi_a$  (b),  $A_{sa}$  (c) and  $\phi_{sa}$  (d) of  $\eta$  determined by tide gauges and AVISO at the closest points to tide gauges (TG) (AVISO – tide gauges). Black bars indicate the differences that pass the significance test, i.e. error bars of two estimated values (one from AVISO and the other from tide gauges) used in comparison do not overlap, while grey bars indicate the insignificant differences.

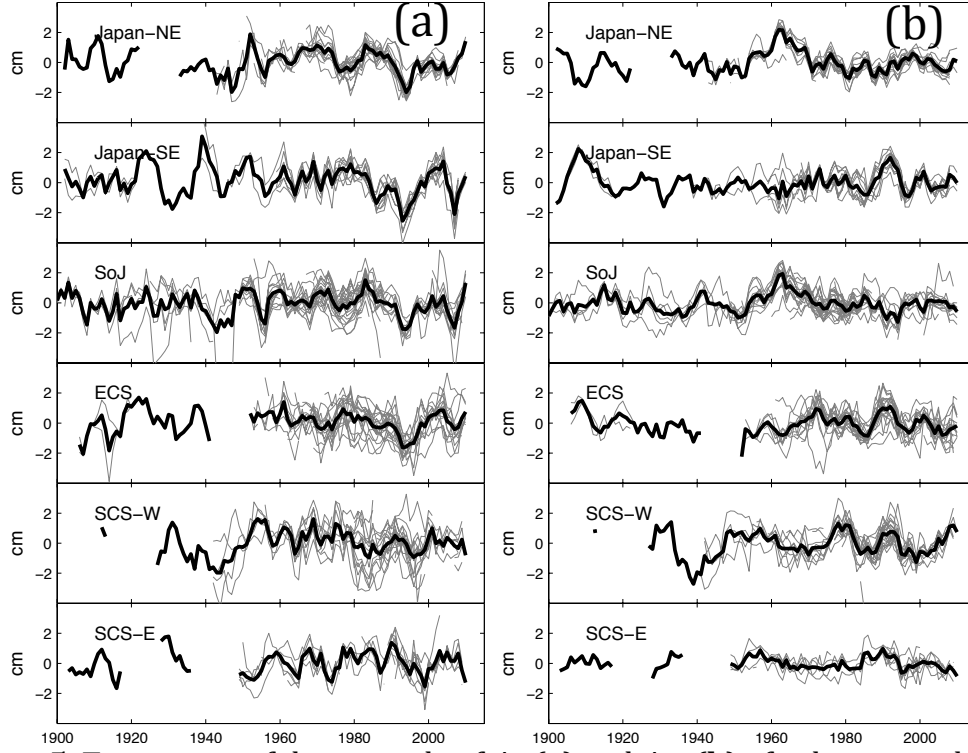


**Figure 5.** Time series of the anomaly of  $A_a$  (a) and  $A_{sa}$  (b) of  $\eta$  determined from tide gauges, which are grouped by 6 sub-regions as specified in **Figure 1**. Bold black line is plotted for the regional ensemble average of individual anomalies in each sub-region.

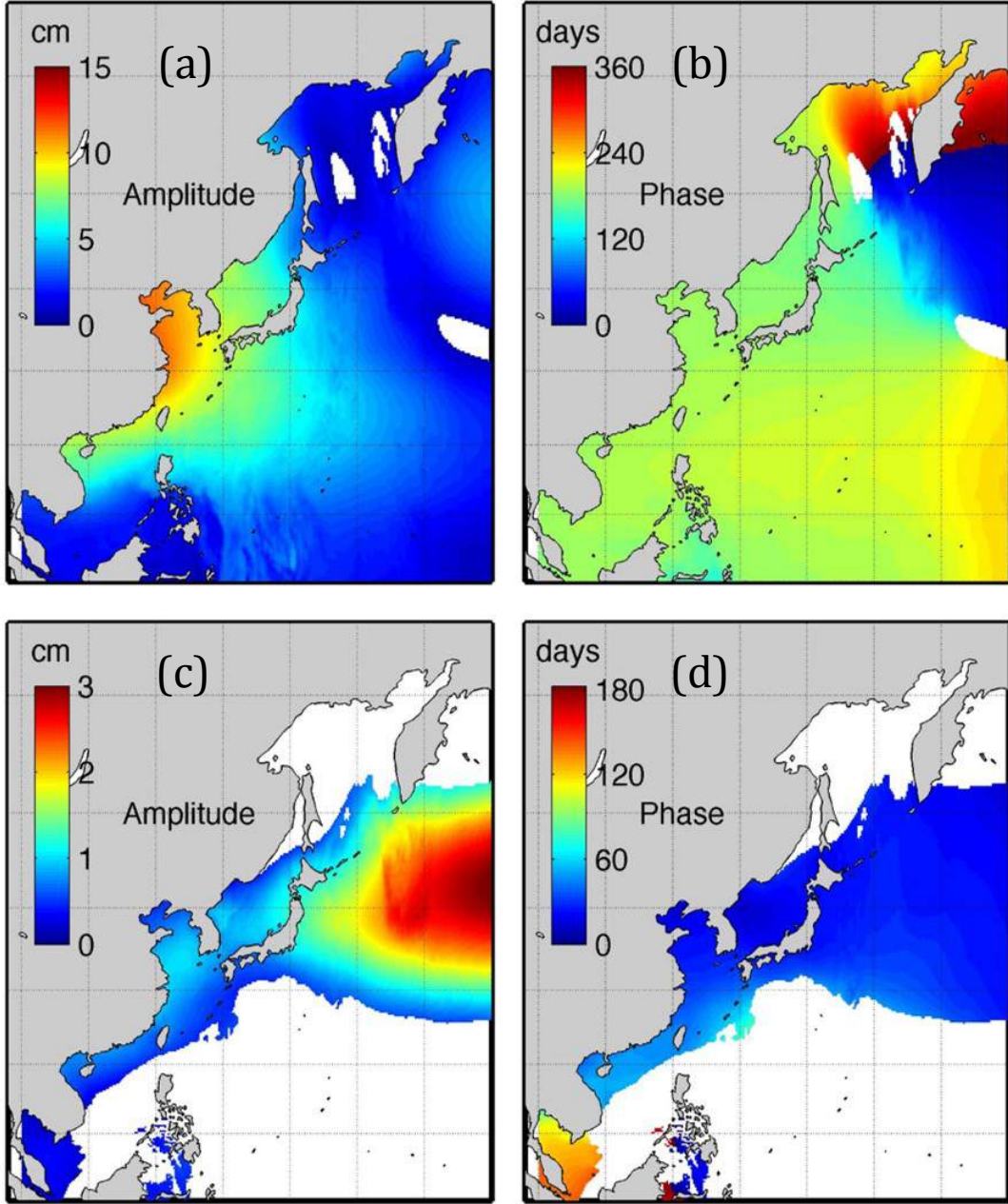


**Figure 6.** Mean  $A_a$  (a),  $\phi_a$  (b),  $A_{sa}$  (c) and  $\phi_{sa}$  (d) for  $\eta_{IB}$  derived from DAC data over 1993-2013. Blank areas indicate the estimates of the annual or semi-annual cycle parameters that are not passing the significance test at 95% confidence level. Please note that the scales of amplitudes here are different from those in **Figure 3**.



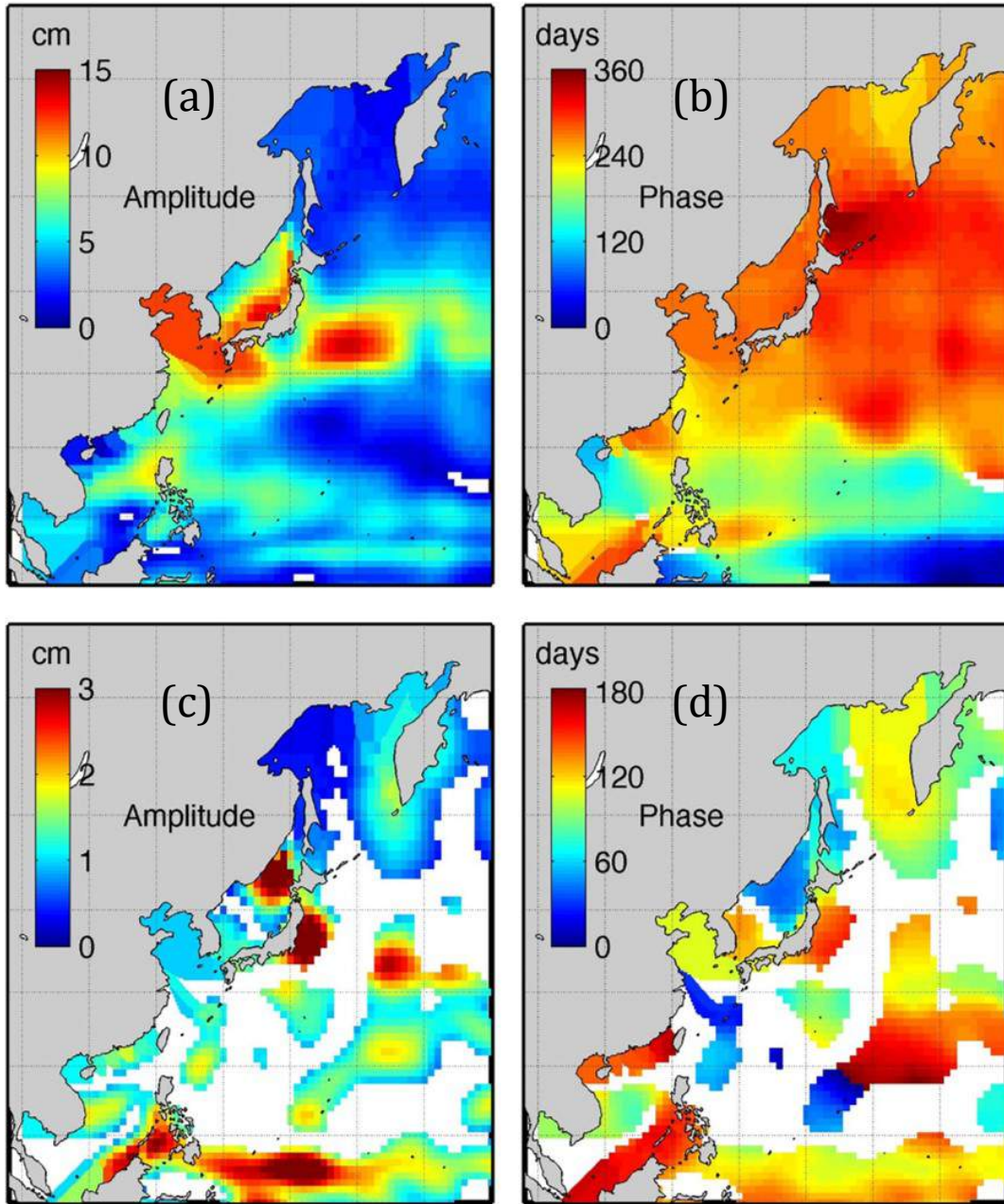


**Figure 7.** Mean  $A_a$  (a),  $\phi_a$  (b),  $A_{sa}$  (c) and  $\phi_{sa}$  (d) for  $\eta_{ster}$  derived from EN4 over 1993-2013. Blank areas indicate the estimates of the annual or semi-annual cycle parameters that are not passing the significance test at 95% confidence level. Please note that the scales of amplitudes here are different from those in **Figure 3**.

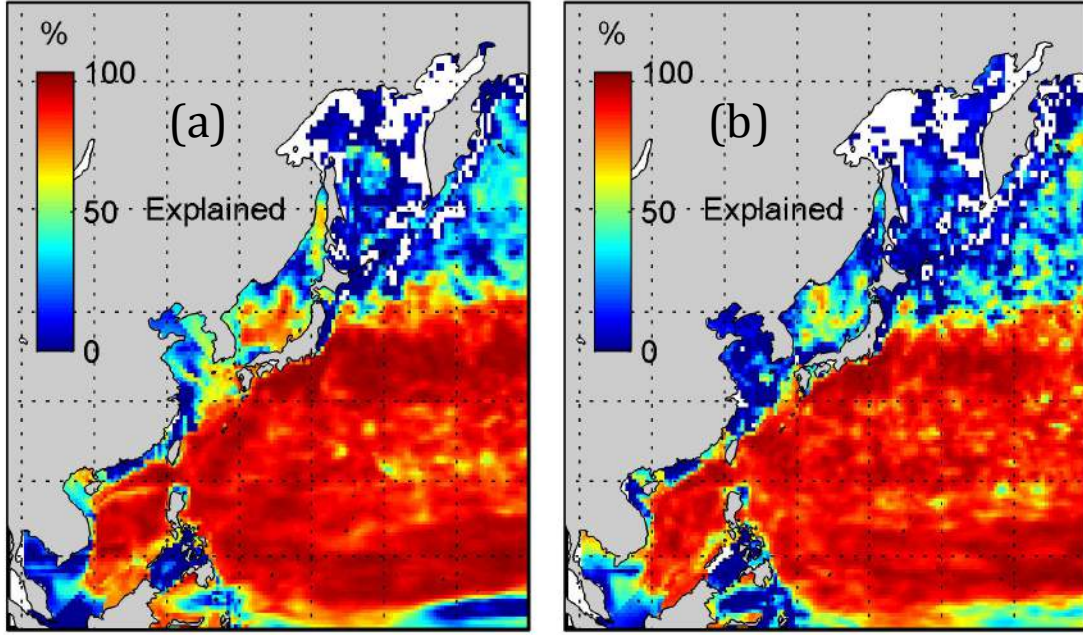


**Figure 8.** Percentage of the inter-annual variability of  $A_a$  (a) and  $A_{sa}$  (b) for  $\eta - \eta_{IB}$  explained by that of  $\eta_{ster}$  over 1900-2010, derived from SODA. Blank areas indicate the grids where the correlation of the inter-annual variability of  $A_a$  or  $A_{sa}$  between  $\eta - \eta_{IB}$  and  $\eta_{ster}$  are not significant at 95% confidence level.



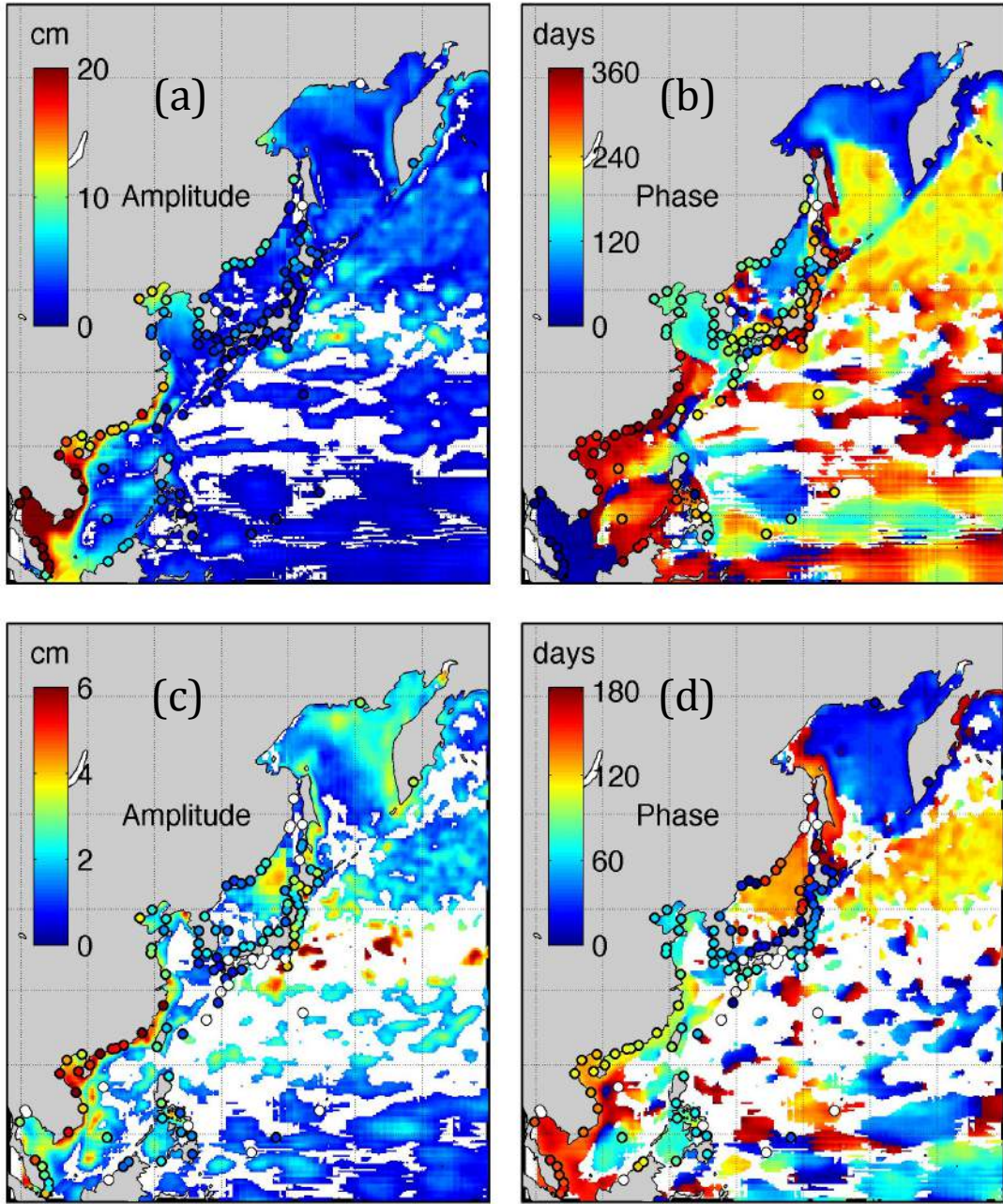


**Figure 9.** Mean  $A_a$  (a),  $\phi_a$  (b),  $A_{sa}$  (c) and  $\phi_{sa}$  (d) for  $\eta - \eta_{IB} - \eta_{ster}$  when  $\eta_{IB}$  and  $\eta_{ster}$  are removed from  $\eta$  provided by tide gauges and AVISO. Blank circles and areas indicate the estimates of the annual or semi-annual cycle parameters that are not passing the significance test at 95% confidence level.

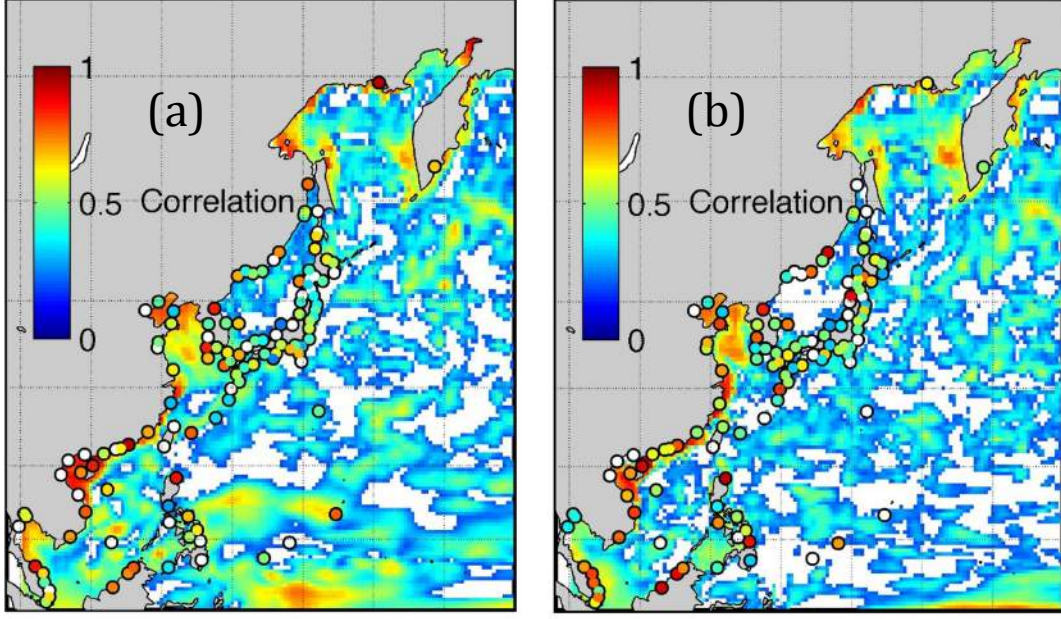


**Figure 10.** (a) Best correlation coefficients of the inter-annual variability of  $A_a$  between  $\eta - \eta_{IB}$ , provided by tide gauges and SODA, and the nearby wind stress; (b) same as (a), but for the correlations between  $\eta - \eta_{IB} - \eta_{ster}$  and the nearby wind stress. Blank circles and areas indicate the correlations that do not pass the significance test at 95% confidence level. Note that the direction of wind stress corresponding to the best correlation coefficients is provided in the supplementary material **Figure S7**.

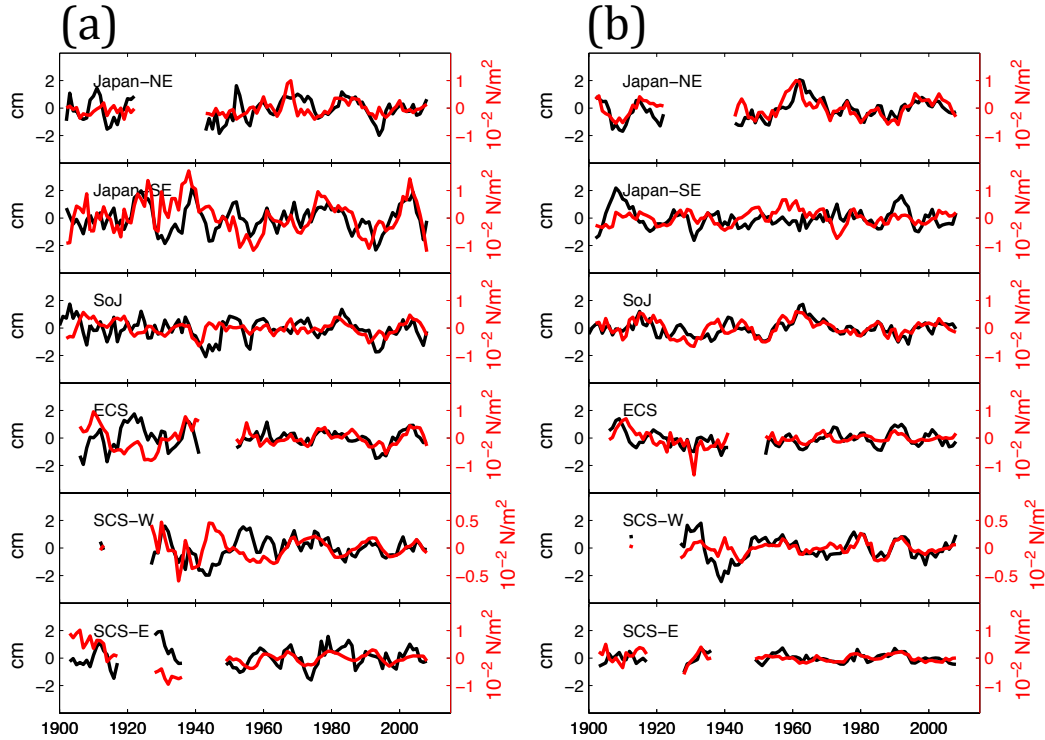


**Figure 11.** Time series of regional average anomaly of  $A_a$  (a) and  $A_{sa}$  (b) for  $\eta - \eta_{IB}$  (black) against the corresponding average of the wind stress (red) in 6 sub-regions as specified in **Figure 1**.



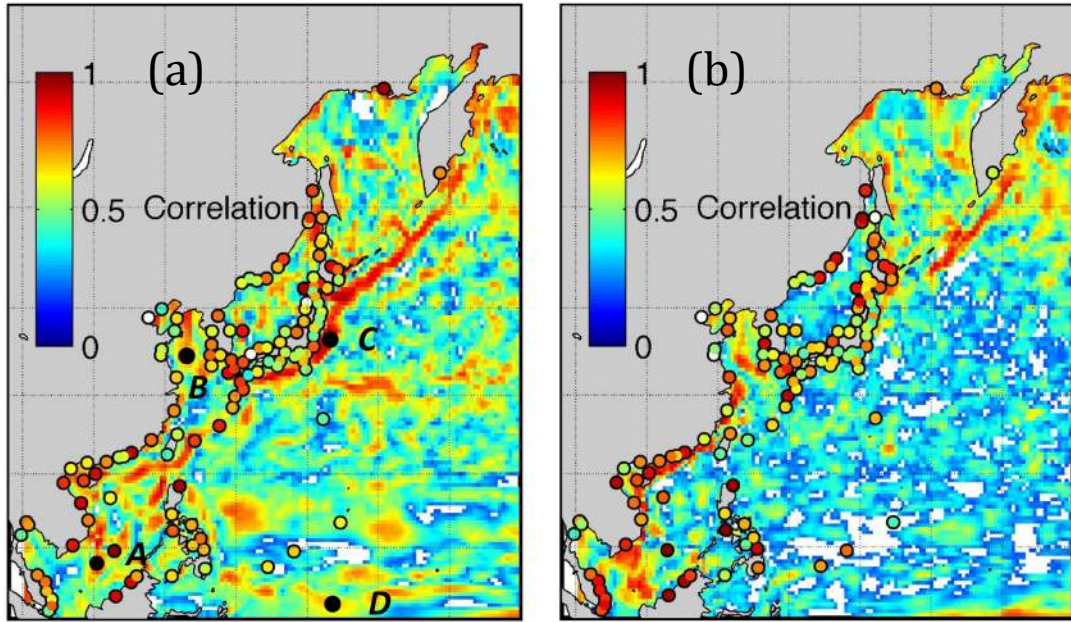


**Figure 12.** Same as **Figure 10**, but for best correlations with the nearby sea surface currents. Black dots in (a) highlight 4 grid points: A [ $8^{\circ}\text{N}$ ,  $108^{\circ}\text{E}$ ], B [ $38^{\circ}\text{N}$ ,  $123^{\circ}\text{E}$ ], C [ $37^{\circ}\text{N}$ ,  $143^{\circ}\text{E}$ ] and D [ $4^{\circ}\text{N}$ ,  $143^{\circ}\text{E}$ ]. Note that the direction of surface currents corresponding to the best correlation coefficients with sea level is provided in the supplementary material **Figure S8**.

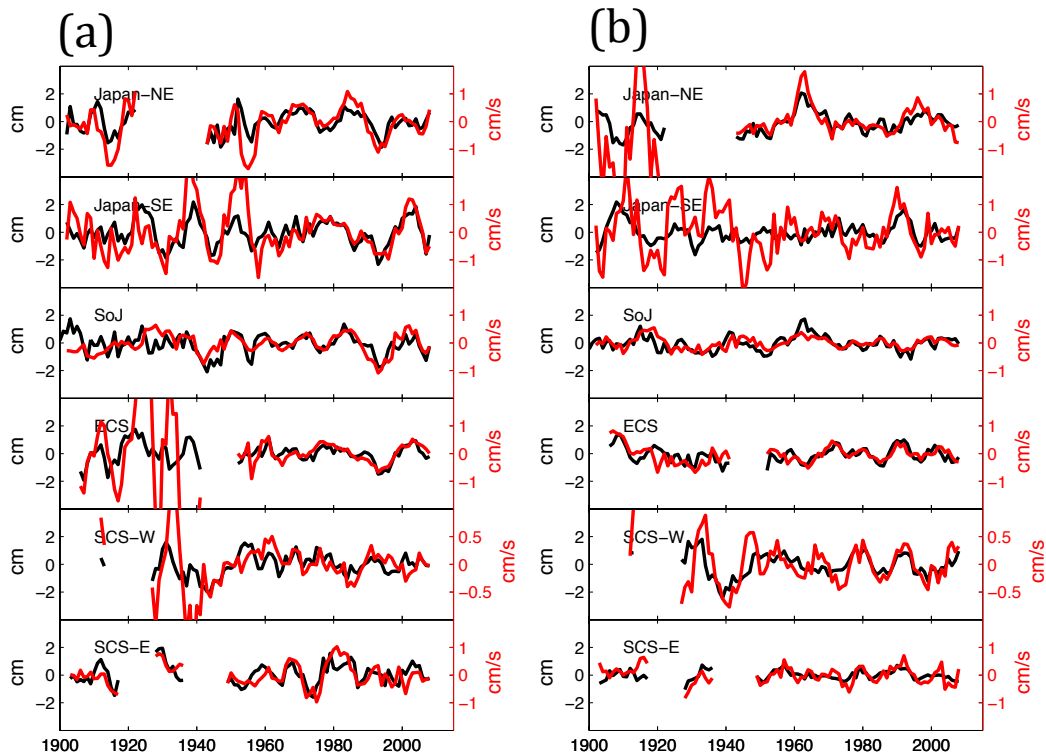


**Figure 13.** Same as **Figure 11**, but for time series of the sea surface currents (red).

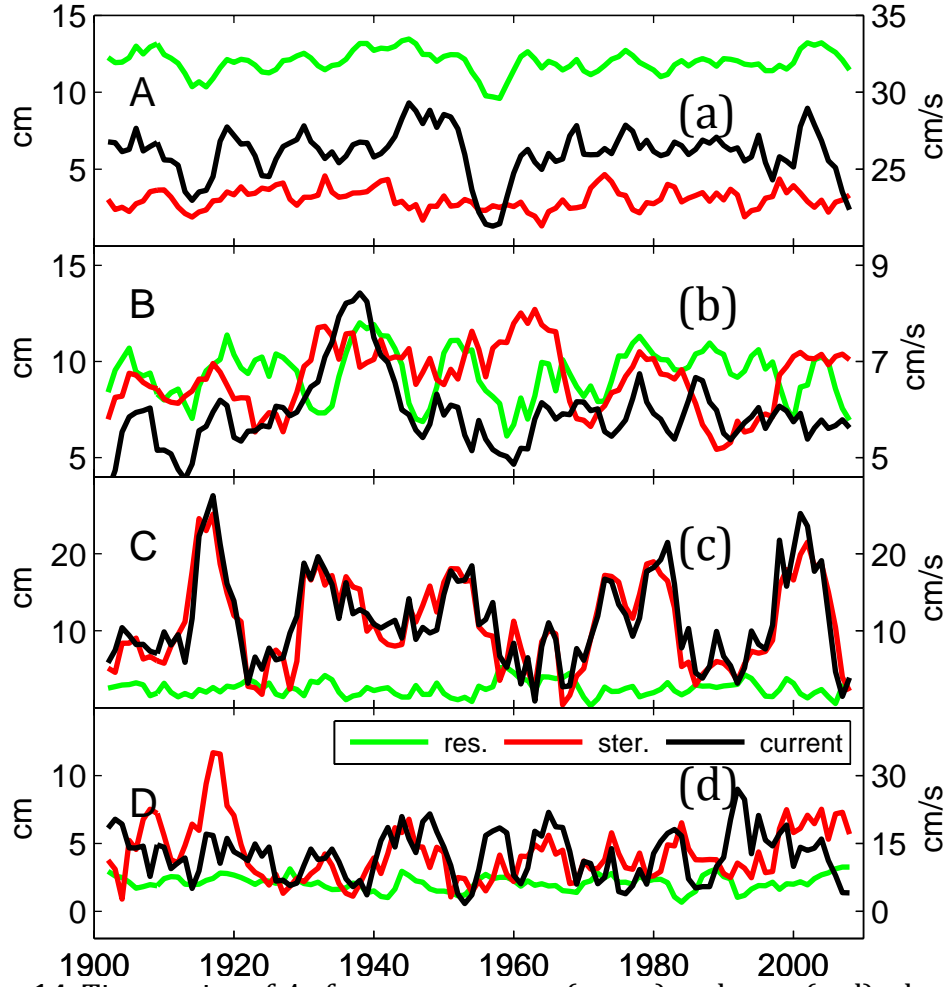
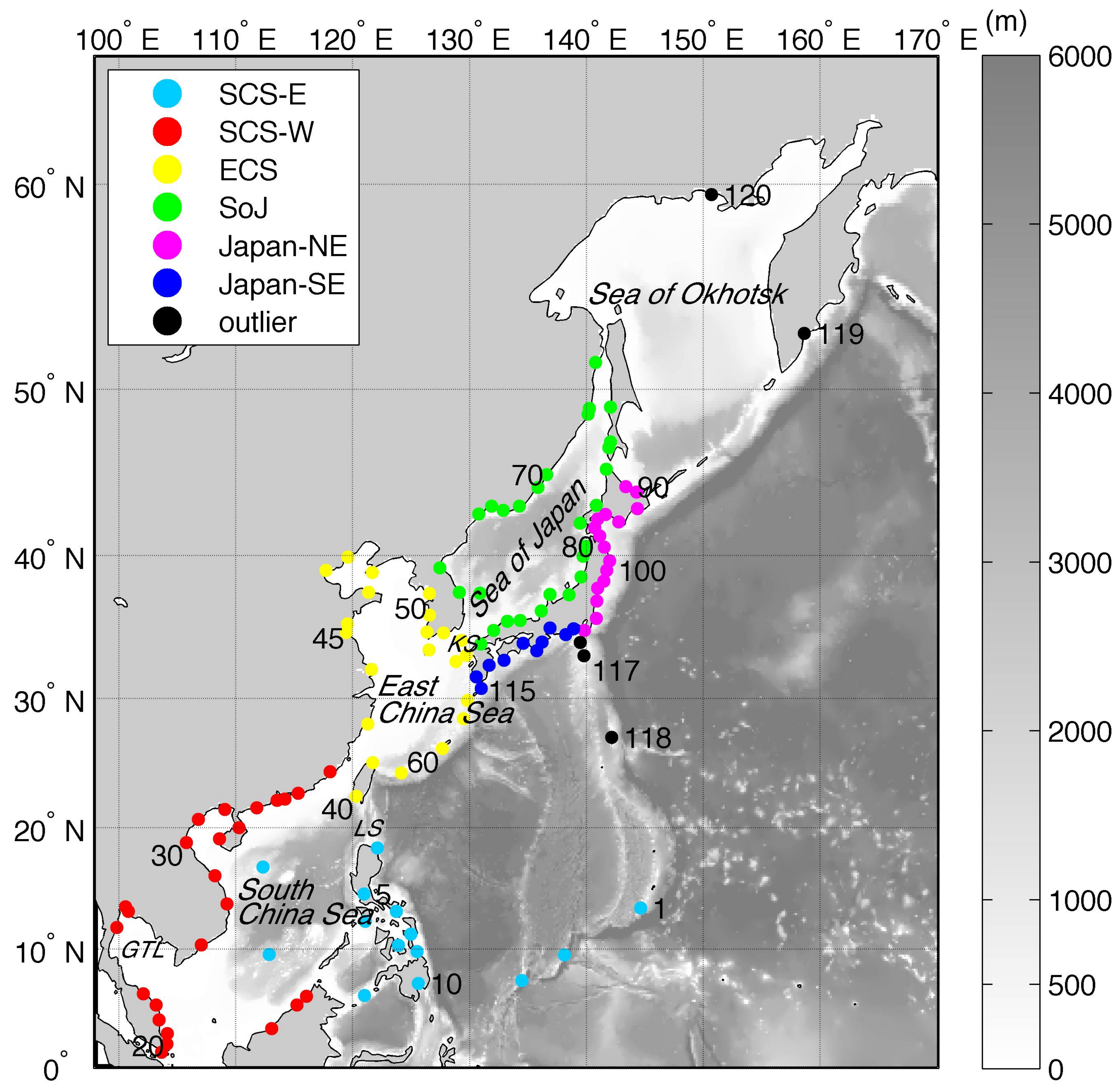


**Figure 14.** Time series of  $A_a$  for  $\eta - \eta_{IB} - \eta_{ster}$  (green) and  $\eta_{ster}$  (red), along with the corresponding quantity of the sea surface currents that are best corrected with time series for  $\eta - \eta_{IB}$ , at 4 grid points A-D (a-d) as indicated in **Figure 12a**.







station number

